

Crystallography

Materials Science and Metallurgy

H. K. D. H. Bhadeshia

Good practice: become familiar the appropriate part of the contents before each lecture. Test your understanding of each lecture using the on-line quizzes.

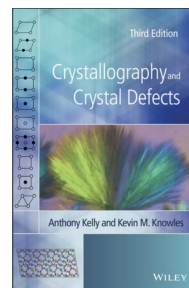
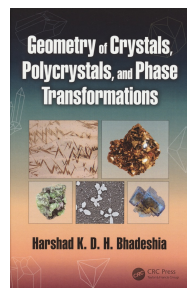
PDF files, slide presentations, videos of lectures, some answers to examination questions, and other materials available on:

www.phase-trans.msm.cam.ac.uk/teaching.html

The PDF version of these notes has hyperlinks which lead to movies making it easier to visualise certain operations.

The books relevant for this course (Tripos reference shelves, library) are:

- Geometry of crystals, polycrystals and phase transformations, 2017, H. K. D. H. Bhadeshia. Electronic version can be downloaded free from:
www.phase-trans.msm.cam.ac.uk/2020/Crystallography_book.pdf
- Crystallography and crystal defects, 3rd edition 2020, A. Kelly and K. M. Knowles



Contents

1	Introduction and Point Groups	5
2	Stereographic Projections	19
3	Stereograms for Low Symmetry Systems	33
4	Space Groups	39
5	The Reciprocal Lattice and Diffraction	45
6	Deformation and Texture	53
7	Interfaces, Orientation Relationships	63
8	Crystallography of Martensitic Transformations	73

Chapter 1

Introduction and Point Groups

1.1 Introduction

Amorphous solids are homogeneous and isotropic because there is no long range order or periodicity in their internal atomic arrangement. In contrast, the crystalline state is characterised by a regular arrangement of atoms over large distances. Crystals are therefore anisotropic – their properties vary with direction. For example, the interatomic spacing varies with orientation within the crystal, as does the elastic response to an applied stress. Note that crystals can be solid or liquid, and can have arbitrary shapes.

Engineering materials are usually aggregates of many crystals of varying sizes and shapes; these *polycrystalline* materials have properties which depend on the nature of the individual crystals, but also on aggregate properties such as the size and shape distributions of the crystals, and the orientation relationships between the individual crystals. The randomness in the orientation of the crystals is a measure of *texture*, which for reasons described later, has to be controlled in the manufacture of transformer steels, uranium fuel rods and beverage cans.

The crystallography of interfaces connecting adjacent crystals can determine the deformation behaviour of the polycrystalline aggregate; it can also influence the toughness through its effect on the degree of segregation of impurities to such interfaces.

1.2 The Lattice

Crystals have translational symmetry: it is possible in a crystal, to identify a regular set of points, known as the lattice points, each of which has an identical environment.

The set of these lattice points constitutes a three dimensional lattice. A *unit cell* may be defined within this lattice as a space-filling parallelepiped with origin at a lattice point, and with its edges given by three non-coplanar *basis vectors* \mathbf{a}_1 , \mathbf{a}_2 and \mathbf{a}_3 , each of which represents translations between two adjacent lattice points. The entire lattice can then be generated by stacking unit cells in three dimensions. Any vector representing a translation between lattice points is called a *lattice vector*.

The unit cell defined above has lattice points located at its corners. Since these are shared with seven other such cells, and since each cell has eight corners, there is only one lattice point per unit cell. Such a unit cell is *primitive* and has the lattice symbol P .

Non-primitive unit cells can have two or more lattice points, in which case, the additional ones will be located at positions other than the corners of the cell. A cell with additional lattice points located at the centres of all its faces has the lattice symbol F ; such a cell would contain four lattice points. Not all the faces of the cell need to have face-centering lattice points; when a cell containing two lattice points has the additional point located at the centre of the face defined by \mathbf{a}_2 and \mathbf{a}_3 , the lattice symbol is A and the cell is said to be A -centred. B -centred and C -centred cells have the additional lattice point located on the face defined by \mathbf{a}_3 & \mathbf{a}_1 or \mathbf{a}_1 & \mathbf{a}_2 respectively. A unit cell with two lattice points can alternatively have the additional lattice point at the body-centre of the cell, in which case the lattice symbol is I . The lattice symbol R is for a trigonal cell; the cell is usually defined such that it contains three lattice points.

The basis vectors \mathbf{a}_1 , \mathbf{a}_2 and \mathbf{a}_3 define the unit cell; their magnitudes a_1 , a_2 and a_3 respectively, are the *lattice parameters* of the unit cell. The angles $\widehat{\mathbf{a}_1 \mathbf{a}_2}$, $\widehat{\mathbf{a}_2 \mathbf{a}_3}$ and $\widehat{\mathbf{a}_3 \mathbf{a}_1}$ are conventionally labelled γ , α and β respectively.

Our initial choice of the basis vectors was arbitrary since there are an infinite number of lattice vectors which could have been used in defining the unit cell. The preferred choice includes small basis vectors which are as equal as possible, provided the shape of the cell reflects the essential symmetry of the lattice.

1.3 Bravais Lattices

The number of ways in which points can be arranged regularly in three dimensions, such that the stacking of unit cells fills space, is not limitless; Bravais showed in 1848 that all possible arrangements can be represented by just fourteen lattices.

The fourteen Bravais lattices can be categorised into seven *crystal systems* (cubic, tetragonal, orthorhombic, trigonal, hexagonal, monoclinic and triclinic, Table 1.1); the cubic system contains for example, the cubic- P , cubic- F and cubic- I lattices. Each crystal system can be characterised uniquely by a set of defining symmetry elements, which any crystal within that system must possess as a minimum requirement (Table 1.1). The Bravais lattices are illustrated in Fig. 1.1.

Table 1.1: The crystal systems. The symmetry axes monad, diad, triad, tetrad and hexad involve rotations of 360° , 180° , 120° , 90° and 60° respectively. These particular rotations leave the lattice in a state that cannot be distinguished from its starting configuration. a_i are the magnitudes of the basis vectors \mathbf{a}_i .

System	Conventional unit cell		Defining symmetry
Triclinic	$a_1 \neq a_2 \neq a_3$	$\alpha \neq \beta \neq \gamma$	monad
Monoclinic	$a_1 \neq a_2 \neq a_3$	$\alpha = \gamma, \beta \geq 90^\circ$	1 diad
Orthorhombic	$a_1 \neq a_2 \neq a_3$	$\alpha = \beta = \gamma = 90^\circ$	3 diads
Tetragonal	$a_1 = a_2 \neq a_3$	$\alpha = \beta = \gamma = 90^\circ$	1 tetrad
Trigonal	$a_1 = a_2 = a_3$	$\alpha = \beta = \gamma \neq 90^\circ$	1 triad
Hexagonal	$a_1 = a_2 \neq a_3$	$\alpha = \beta = 90^\circ, \gamma = 120^\circ$	1 hexad
Cubic	$a_1 = a_2 = a_3$	$\alpha = \beta = \gamma = 90^\circ$	4 triads

1.4 Directions

Any vector \mathbf{u} can be represented as a linear combination of the basis vectors \mathbf{a}_i of the unit cell ($i = 1, 2, 3$):

$$\mathbf{u} = u_1\mathbf{a}_1 + u_2\mathbf{a}_2 + u_3\mathbf{a}_3 \quad (1.1)$$

and the scalar quantities u_1 , u_2 and u_3 are the components of the vector \mathbf{u} with respect to the basis vectors \mathbf{a}_1 , \mathbf{a}_2 and \mathbf{a}_3 . Once the unit cell is defined, any direction \mathbf{u} within the lattice can be identified uniquely by its components $[u_1 \ u_2 \ u_3]$, and the components are called the Miller indices of that direction and are by convention enclosed in square brackets (Fig. 1.3).

It is sometimes the case that the properties along two or more different directions are identical. These directions are said to be *equivalent* and the crystal is said to possess *symmetry*. For example, the $[1 \ 0 \ 0]$ direction for a cubic lattice is equivalent to the $[0 \ 1 \ 0]$, $[0 \ 0 \ 1]$, $[0 \ \bar{1} \ 0]$, $[0 \ 0 \ \bar{1}]$ and $[\bar{1} \ 0 \ 0]$ directions; the bar on top of the number implies that the index is negative.

The indices of directions of the same form are conventionally enclosed in special brackets, *e.g.* $\langle 1 \ 0 \ 0 \rangle$. The number of equivalent directions within the form is called the multiplicity of that direction, which in this case is 6.

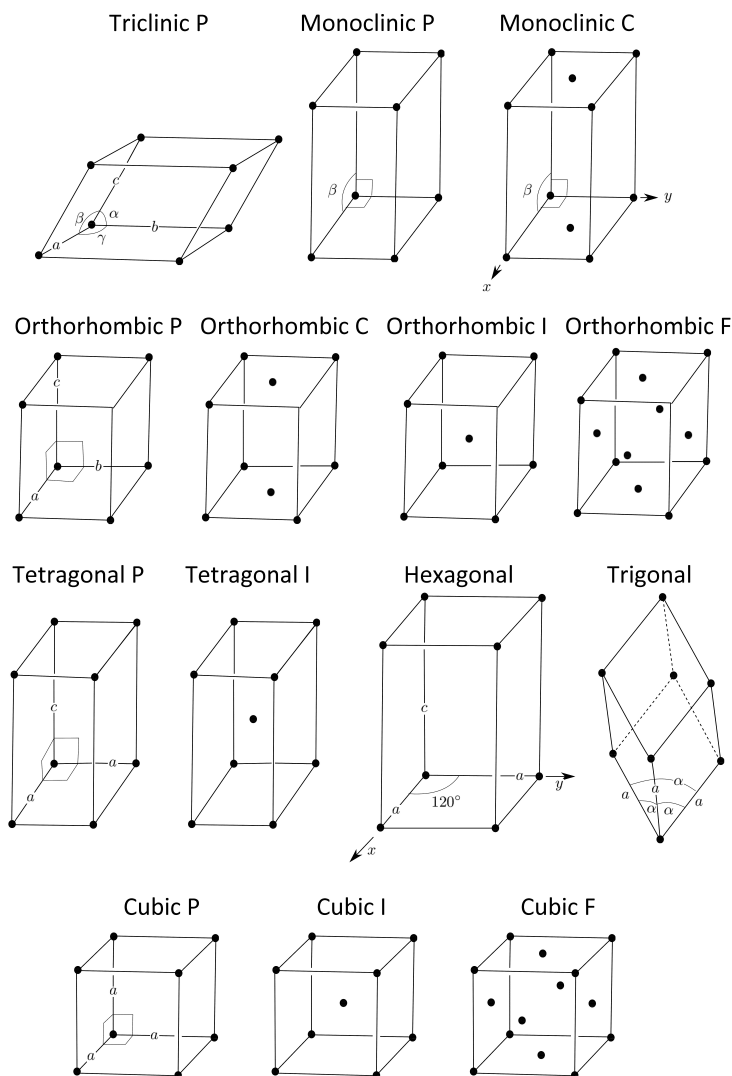


Figure 1.1: The fourteen three-dimensional Bravais lattices.

1.5 Planes

If a plane intersects the \mathbf{a}_1 , \mathbf{a}_2 and \mathbf{a}_3 axes at distances x_1 , x_2 and x_3 respectively, relative to the origin, then the Miller indices of that plane are given by $(h_1 h_2 h_3)$ where:

$$h_1 = \phi a_1/x_1, \quad h_2 = \phi a_2/x_2, \quad h_3 = \phi a_3/x_3 \quad (1.2)$$

ϕ is a scalar which clears the numbers h_i off fractions or common factors. Note that x_i are negative when measured in the $-\mathbf{a}_i$ directions. The intercept of the plane with an axis may occur at ∞ , in which case the plane is parallel to that axis and the corresponding Miller index will be zero (Fig. 1.3).

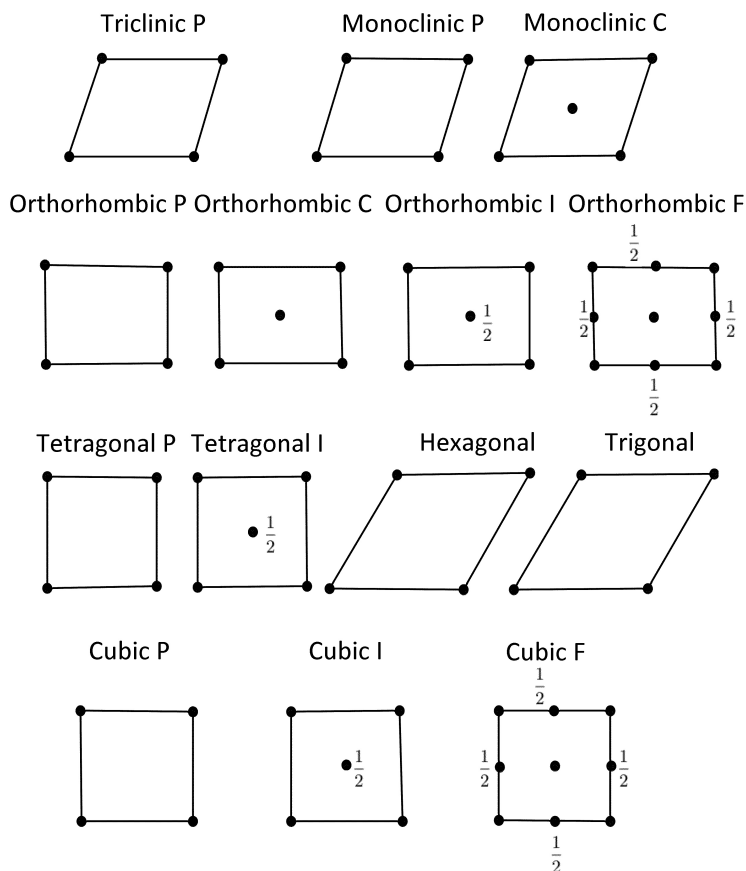


Figure 1.2: Projection of the three-dimensional shapes of the fourteen Bravais lattices on to the \mathbf{a}_1 - \mathbf{a}_2 plane. The numbers indicate the coordinates of lattice points relative to the \mathbf{a}_3 axis; the unlabelled lattice points are by implication located at coordinates 0 and 1 with respect to the \mathbf{a}_3 axis.

Miller indices for planes are by convention written using round brackets: $(h_1 h_2 h_3)$ with braces being used to indicate planes of the same form: $\{h_1 h_2 h_3\}$.

1.6 Weiss Zone Law

This law states that if a direction $[u_1 u_2 u_3]$ lies in a plane $(h_1 h_2 h_3)$ then

$$u_1 h_1 + u_2 h_2 + u_3 h_3 = 0 \quad (1.3)$$

and the law applies to any crystal system. We shall prove this when we deal with the reciprocal lattice.

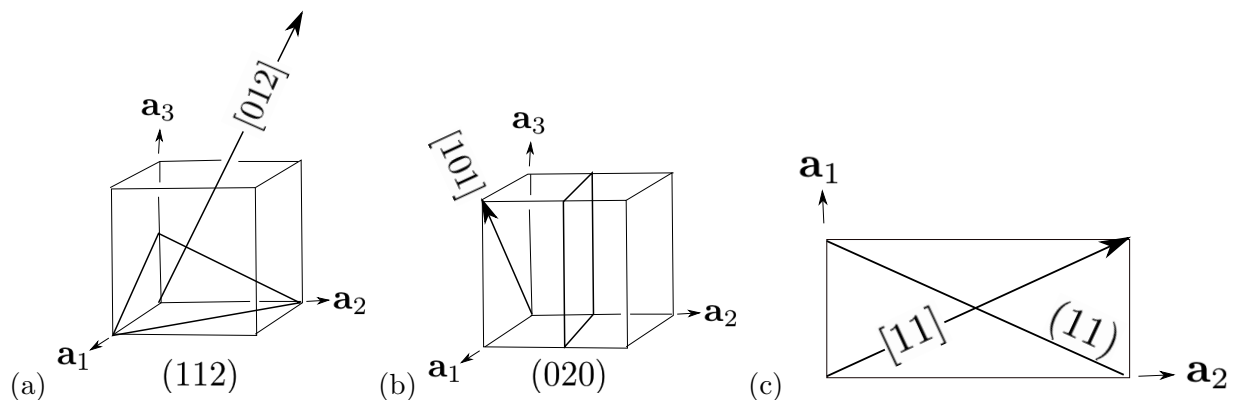


Figure 1.3: (a,b) Miller indices for directions and planes. (c) Notice that in non-cubic systems, a direction with indices identical to those of a plane is not necessarily normal to that plane.

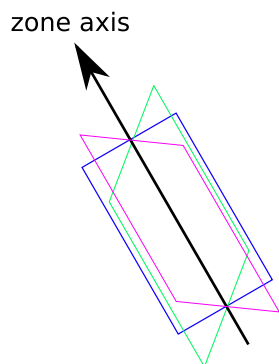


Figure 1.4: A *zone* refers to a set of planes which share a common direction, which in turn is known as a zone axis. The direction illustrated would satisfy the Weiss law for all the planes shown. For example, the planes $(1\ 1\ 1)$, $(1\ 1\ 2)$ and $(1\ 1\ 0)$ all belong to the zone $[1\ \bar{1}\ 0]$.

1.7 Symmetry

Although the properties of a crystal can be anisotropic, there may be different directions along which they are identical. These directions are said to be *equivalent* and the crystal is said to possess *symmetry*.

That a particular edge of a cube cannot be distinguished from any other is a measure of its symmetry; an orthorhombic parallelepiped has lower symmetry, since its edges can be distinguished by length.

Some symmetry operations are illustrated in Fig. 1.5; in essence, they transform a spatial arrangement into another that is indistinguishable from the original. The rotation of a cubic lattice through 90° about an axis along the edge of the unit cell is an example of a symmetry operation, since the lattice points of the final and original lattice coincide in space and cannot consequently be distinguished.

We have implicitly encountered translational symmetry when defining the lattice; since the envi-

ronment of each lattice point is identical, translation between lattice points has the effect of shifting the origin.

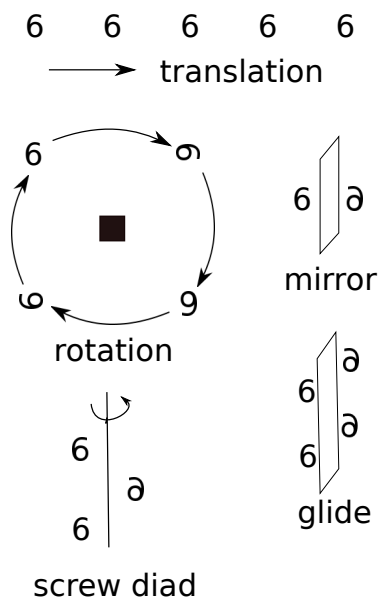


Figure 1.5: Some symmetry operations. The mirror plane involves reflection symmetry, whereas the glide plane is a combination of reflection and translation parallel to the mirror. Translational symmetry is intrinsic to all lattices whereas the other elements may or may not exist for all lattices. For example, the triclinic lattice has no mirror or glide plane.

Note that the translations involved in the screw axis and glide plane are rational fractions of the repeat distance along the translation direction. The screw axis illustrated involves a rotation of 180° (\equiv diad) combined with a translation parallel to the axis.

1.8 Symmetry Operations

An object possesses an n -fold axis of rotational symmetry if it coincides with itself upon rotation about the axis through an angle $360^\circ/n$. The possible angles of rotation, which are consistent with the translational symmetry of the lattice, are 360° , 180° , 120° , 90° and 60° for values of n equal to 1, 2, 3, 4 and 6 respectively. A five-fold axis of rotation does not preserve the translational symmetry of the lattice and hence is forbidden. A one-fold axis of rotation is called a monad and the terms diad, triad, tetrad and hexad correspond to $n = 2, 3, 4$ and 6 respectively.

All of the Bravais lattices have a *centre of symmetry*, Fig. 1.6. An observer at the centre of symmetry sees no difference in arrangement between the directions $[u_1 u_2 u_3]$ and $[-u_1 -u_2 -u_3]$. The centre of symmetry is such that inversion through that point produces an identical arrangement but in the opposite sense. A *rotoinversion* axis of symmetry rotates a point through a specified angle and then inverts it through the centre of symmetry such that the arrangements before and after this combined operation are in coincidence. For example, a three-fold inversion axis involves a rotation through 120° combined with an inversion, the axis being labelled $\bar{3}$.

A rotation operation can also be combined with a translation parallel to that axis to generate a *screw axis* of symmetry. The magnitude of the translation is a fraction of the lattice repeat distance along the axis concerned. A 3_1 screw axis would rotate a point through 120° and translate it through a distance $t/3$, where t is the magnitude of the shortest lattice vector along the axis. A 3_2 operation involves a rotation through 120° followed by a translation through $2t/3$ along the

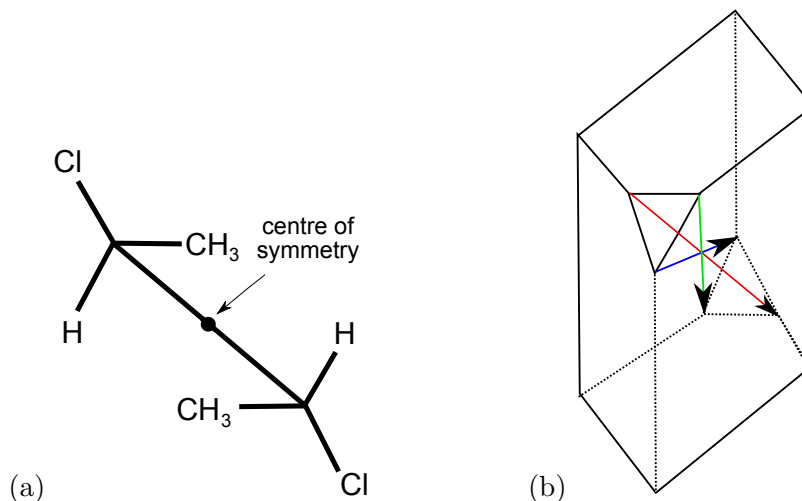


Figure 1.6: Illustration of centre of symmetry. (a) A molecule with the centre of symmetry identified by the dot. (b) The common point where the arrows intersect is the centre of symmetry.

axis. For a right-handed screw axis, the sense of rotation is anticlockwise when the translation is along the positive direction of the axis.

A plane of *mirror symmetry* implies arrangements which are mirror images. Our left and right hands are (approximately) mirror images. The operation of a $\bar{2}$ axis produces a result which is equivalent to a reflection through a mirror plane normal to that axis.

The operation of a *glide plane* combines a reflection with a translation parallel to the plane, through a distance which is half the lattice repeat in the direction concerned. The translation may be parallel to a unit cell edge, in which case the glide is *axial*; the term *diagonal* glide refers to translation along a face or body diagonal of the unit cell. In the latter case, the translation is through a distance which is half the length of the diagonal concerned, except for *diamond* glide, where it is a quarter of the diagonal length.

1.9 Crystal Structure

Lattices are regular arrays of imaginary points in space. A real crystal has atoms associated with these points. Consider the projection of the primitive cubic cell illustrated in Fig. 1.7a. In the sequence Fig. 1.7b-e, a pair of atoms (Cu at 0,0,0 and Zn at $\frac{1}{2}, \frac{1}{2}, \frac{1}{2}$), which also is known as the *motif*, is placed at each lattice point of Fig. 1.7a in order to build up the crystal structure of β -brass (Fig. 1.7f).

$$\text{lattice} + \text{motif} = \text{crystal structure} \quad (1.4)$$

The location of an atom of copper at each lattice point of a cubic- F lattice, generates the crystal

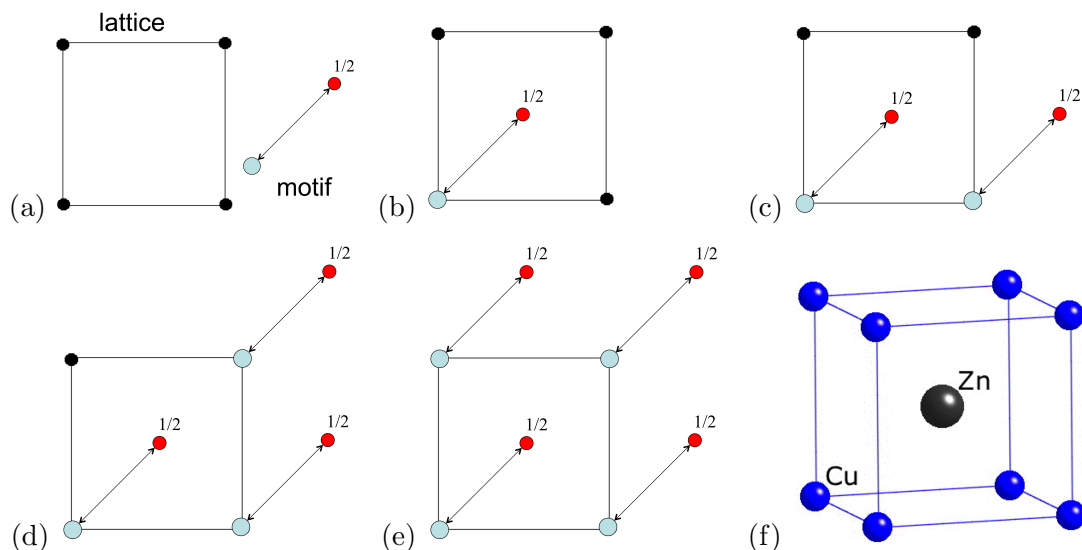


Figure 1.7: Building up the crystal structure of β -brass by placing a motif consisting of an appropriate pair of Cu and Zn atoms at each lattice point of a primitive cubic lattice. (a) represents the primitive lattice with the motif consisting of a pair of distinct atoms that have yet to be placed. (b-e) The motif is placed at each lattice point. (f) The three-dimensional representation of the final structure.

structure of copper, with four copper atoms per unit cell (one per lattice point), representing the actual arrangement of copper atoms in space.

Consider a motif consisting of a pair of carbon atoms, with coordinates $[0\ 0\ 0]$ and $[\frac{1}{4}\ \frac{1}{4}\ \frac{1}{4}]$ relative to a lattice point. Placing this motif at each lattice point of the cubic- F lattice generates the diamond crystal structure (Fig. 1.8), with each unit cell containing 8 carbon atoms (2 carbon atoms per lattice point).

Fig. 1.9 shows how a Cubic- F cell changes into a Cubic- P cell when the nickel and aluminium atoms order in the classical γ/γ' superalloy system.

1.10 Point Group Symmetry

Consider a molecule such as that illustrated in Fig. 1.10. The symmetry operations on the molecule constitute a collection known as a *point group* because there is always one point in space that is left unchanged by every symmetry operation in that group. The point group symmetry of the molecule is illustrated in Fig. 1.10a. When exposed to infrared light the molecules absorb energy and vibrate

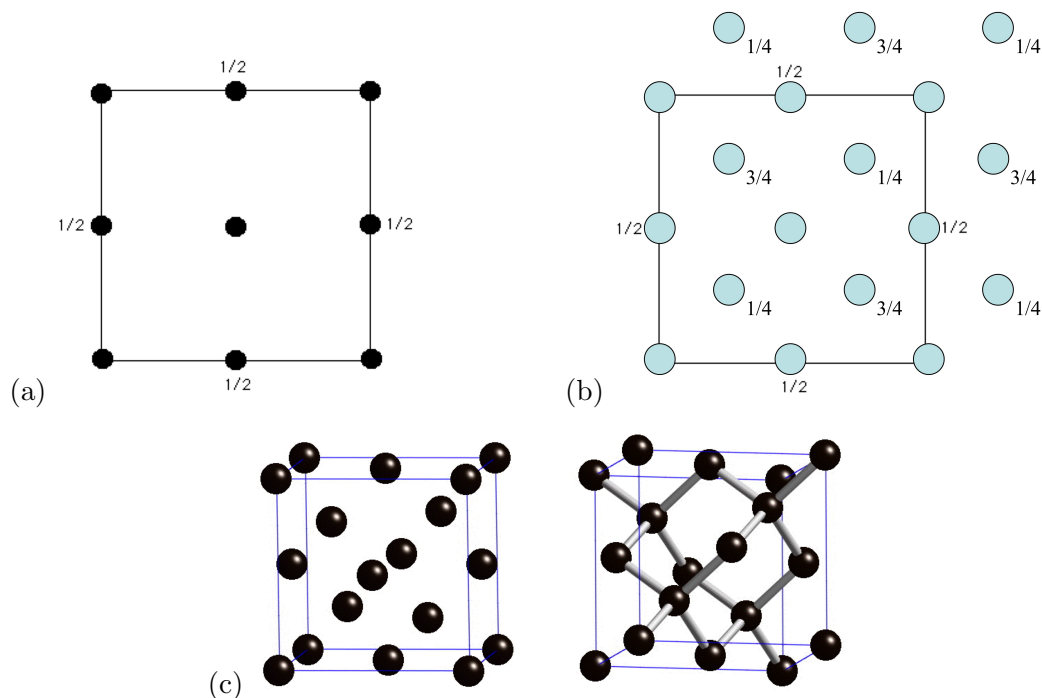


Figure 1.8: (a) Projection of the cubic-F lattice. (b) Projection of cubic-F lattice with a motif of a pair of carbon atoms at $0,0,0$ and $\frac{1}{4}, \frac{1}{4}, \frac{1}{4}$ placed at each lattice point. (c) Perspective of the same structure illustrating the tetrahedral bonding of the carbon atoms.

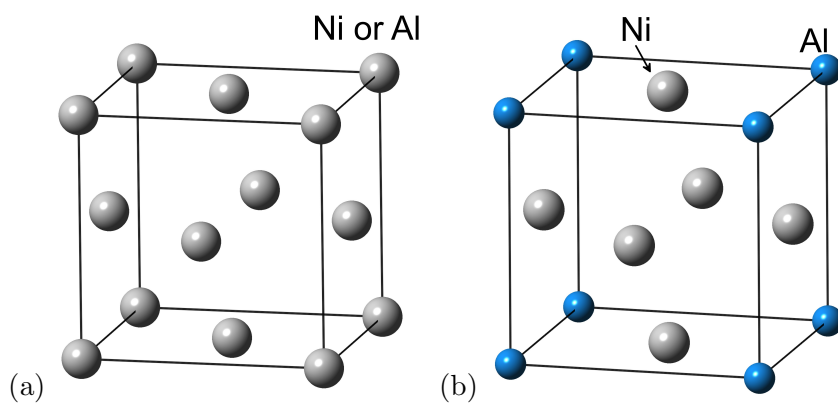


Figure 1.9: Nickel based superalloys. (a) The face-centred cubic crystal structure of disordered γ . (b) The primitive cubic crystal structure of γ' .

as illustrated in Fig. 1.10b. These vibrations result in a characteristic spectrum showing peaks at certain energies which depend on the modes illustrated. Other molecules with the same point group symmetry, such as sulphur tetrafluoride, will exhibit similar spectroscopic properties. The point group of a crystal is also the symmetry common to all of its *macroscopic* properties.

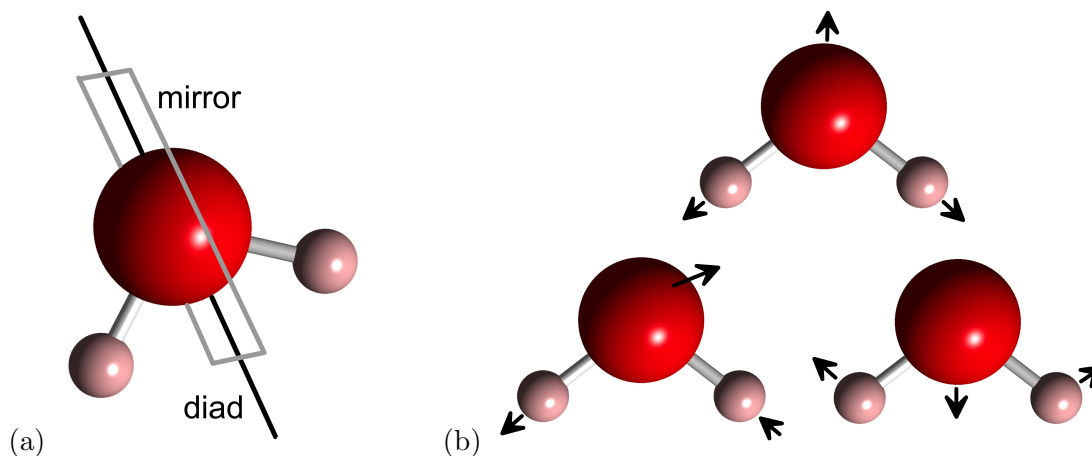


Figure 1.10: (a) A molecule with point group symmetry $2m$ (diad and a mirror plane parallel to the diad). (b) Vibration modes (symmetrical stretch, asymmetrical stretch and bending) of the molecule when appropriately stimulated.

Translations are therefore necessarily excluded in a *point* group. Rotations, mirror planes, centre of symmetry and inversion axes are permitted. There are 32 point groups in three dimensions, classified within the seven crystal classes (Table 1.2). The triclinic, monoclinic and orthorhombic groups do not contain triads, tetrads or hexads. For those systems, when the point group symbol contains three elements (e.g. $2mm$), then the symbols are presented in the order of the symmetry elements parallel to the x , y and z axes respectively, as illustrated in Fig. 1.11a for an object in the orthorhombic class.

For crystal systems with higher order axes, the z direction is assigned to that higher order axis, with the second symbol corresponding to equivalent *secondary* axes that are normal to z , and the third also normal to z to equivalent *tertiary* directions passing between the secondary ones. Fig. 1.11b shows an example for an object in the tetragonal class, with the tetrad placed along the z axis, the two mirror planes with normals along the x and y axes and the additional mirror planes generated by this symmetry also illustrated.

In the case of the cubic system the triad is always the second symbol given that the defining symmetry is four triads.

Some further details on the notation are as follows:

- $m \equiv \bar{2}$ represents a mirror plane.
- 2, 3, 4, 6 are 2-fold, 3-fold, 4-fold and 6-fold rotation axes, respectively.
- $\bar{1}$, $\bar{2}$, $\bar{3}$ etc. are inversion axes; the one fold inversion axis is equivalent to a centre of symmetry; $\bar{2}$ signifies a rotation of $360^\circ/2$ combined with an inversion through the centre point.

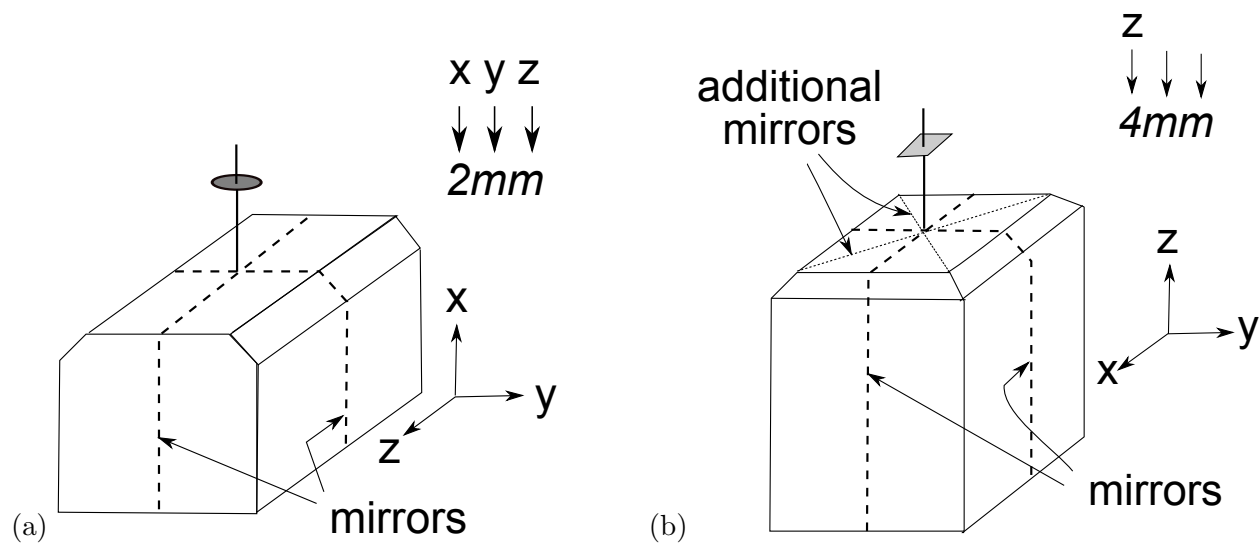


Figure 1.11: Convention for point group notation. (a) Groups without high order axes. (b) Groups with high order axes.

- $\frac{4}{m}mm$ is a 4-fold axis with a mirror normal to it and four mirror planes containing it. The symbol is usually written without the space as $4/mmm$
- 432 refers to a point group with 3-fold axes which are not parallel to the z axis, where a unit cell has x , y and z axes. This is limited to the cubic system.

Table 1.2: Point group symmetries associated with the seven crystal classes.

Class	Non-centrosymmetric	Centrosymmetric	
Cubic	23, 432, $\bar{4}3m$	$m\bar{3}$, $m\bar{3}m$	} With high order axes
Hexagonal	6, $\bar{6}$, 622, $6mm$, $\bar{6}m2$	$6/m$, $6/mmm$	
Trigonal	3, 32, $3m$	$\bar{3}$, $\bar{3}m$	
Tetragonal	4, $\bar{4}$, 422, $4mm$, $\bar{4}2m$	$4/m$, $4/mmm$	
Orthorhombic	222, $2mm$	mmm	} Without high order axes
Monoclinic	2, m	$2/m$	
Triclinic	1	$\bar{1}$	

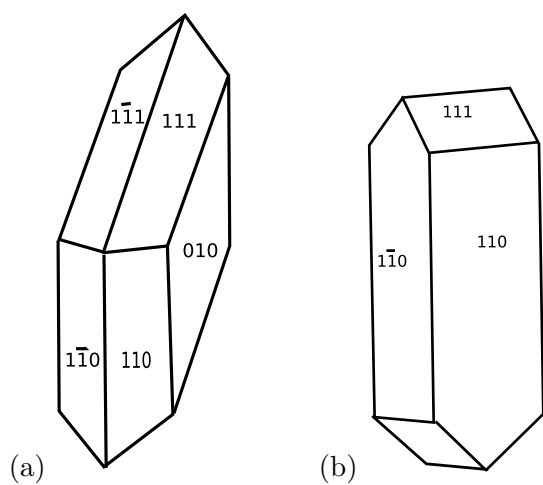


Figure 1.12: (a) Shape of gypsum ($\text{CaSO}_4 \cdot 2\text{H}_2\text{O}$) with point group symmetry $2/m$. (b) Shape of epsomite ($\text{MgSO}_4 \cdot 7\text{H}_2\text{O}$) with point group symmetry 222. Note that the angle between the (110) and ($1\bar{1}0$) faces is 89.37° , because the lattice parameters a , b , and c are 1.1866, 1.1998 and 0.6855 nm respectively.

Chapter 2

Stereographic Projections

2.1 Introduction

We have seen already that the projection of a three-dimensional crystal structure into two dimensions, along the z -coordinate, can simplify the perception and representation of atomic arrangements. There is no loss of information given that the fractional z -coordinate is clearly identified on the projection. This can be seen in Fig. 1.8 where the three dimensional representation of the structure of diamond lacks clarity whereas the projected cell is readily visualised. The ease of interpretation using the projected structure is illustrated for the more complex structure of ε -carbide, which has a chemical formula between Fe_2C and Fe_3C , in Fig. 2.1. There are six iron atoms in the cell (3 at $z = \frac{1}{2}$ and the six others that are shared with other cells at $z = 0, 1$ and therefore contributing a further 3 to the cell). The illustrated cell contains a full complement of carbon atoms but to achieve the composition $\text{Fe}_{2.4}\text{C}$, the sites coloured blue would only be occupied partially.

The projection described in Fig. 2.1 is a straightforward linear operation and there are no distortions of that linearity. In contrast, Fig. 2.2 show non-linear projections of circular arcs, in one case a simple extrapolation on to a horizontal line, and in the other case via a pole located below the horizontal line where the projections are recorded. The purpose here is to record angles rather than spatial coordinates.

Imagine now that instead of quadrants of a circle, the diagrams in Fig. 2.2 represent the surfaces of spheres. A circle drawn on the surface of the sphere would in general project as an ellipse on the horizontal plane of Fig. 2.2a, whereas it would project as a true circle in the case of the projection method used in Fig. 2.2b.

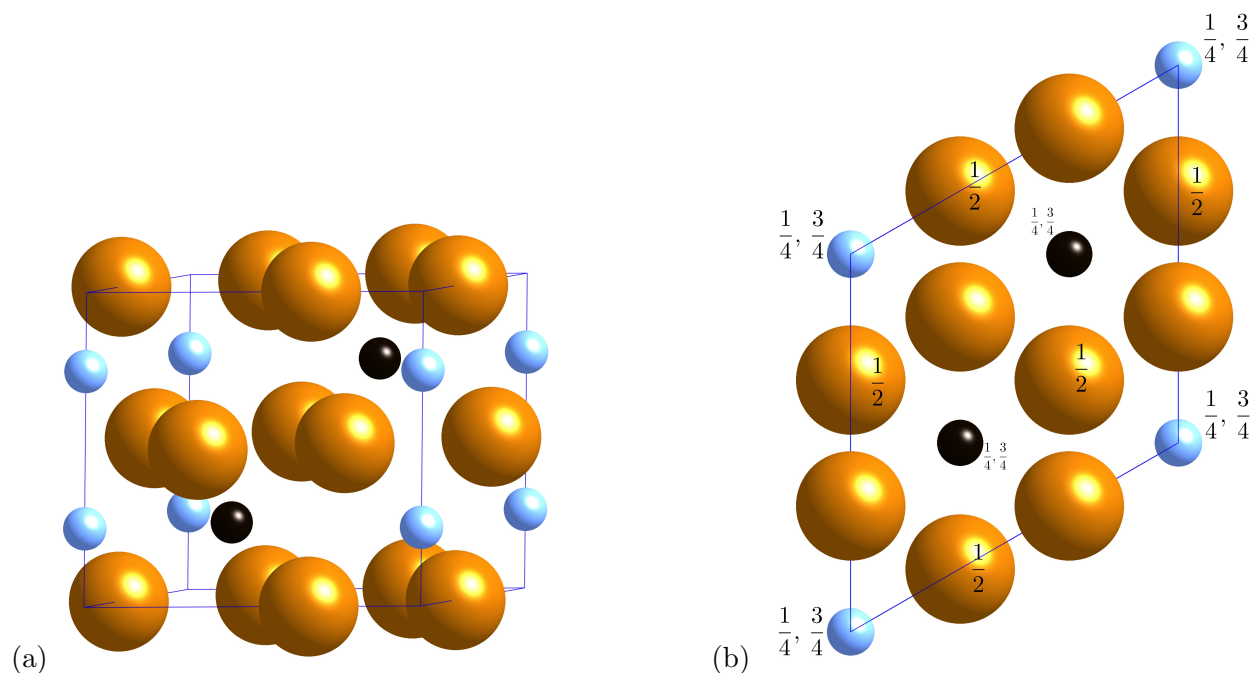


Figure 2.1: The structure of hexagonal ϵ -carbide with lattice parameters $a = 0.4767$ nm and $c = 0.4353$ nm. The large atoms are iron. The small atoms are carbon but not all the sites designated blue are occupied. (a) The three dimensional cell with the z -axis vertical. (b) Projection of the cell along the z -axis, with the fractional z -coordinates listed.

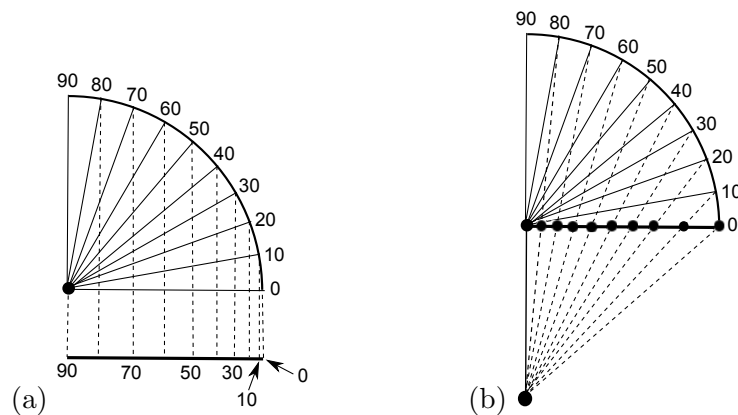


Figure 2.2: Projections of angles made by lines intersecting a circular quadrant onto a horizontal line.

2.2 Angular truth

Consider a sphere that has north and south poles. If a circle is constructed on the northern hemisphere with each point on its locus projected on to the equatorial plane by lines originating

from the south pole, then the projection itself will remain a circle. Fig 2.3a illustrates the circle ab on the surface of the sphere, together with its projection $a'b'$ on the equatorial plane. A cross-section of the same diagram through the centre of the circle ab is shown in Fig 2.3. The conjugate circular section cd is symmetrically inclined to the axis ST .

The line eb is constructed to be parallel to the equatorial plane. The arcs eS and Sb are equal in length so it follows that $\phi_1 = \phi_2$. Since cd is symmetrically inclined to ST , it follows that $\phi_3 = \phi_2$ and therefore $\phi_3 = \phi_1$. In other words, the circle cd is parallel to the equatorial plane. If the circle cd is now translated towards the equatorial plane, it remains a circle and ends up as a circle $a'b'$.

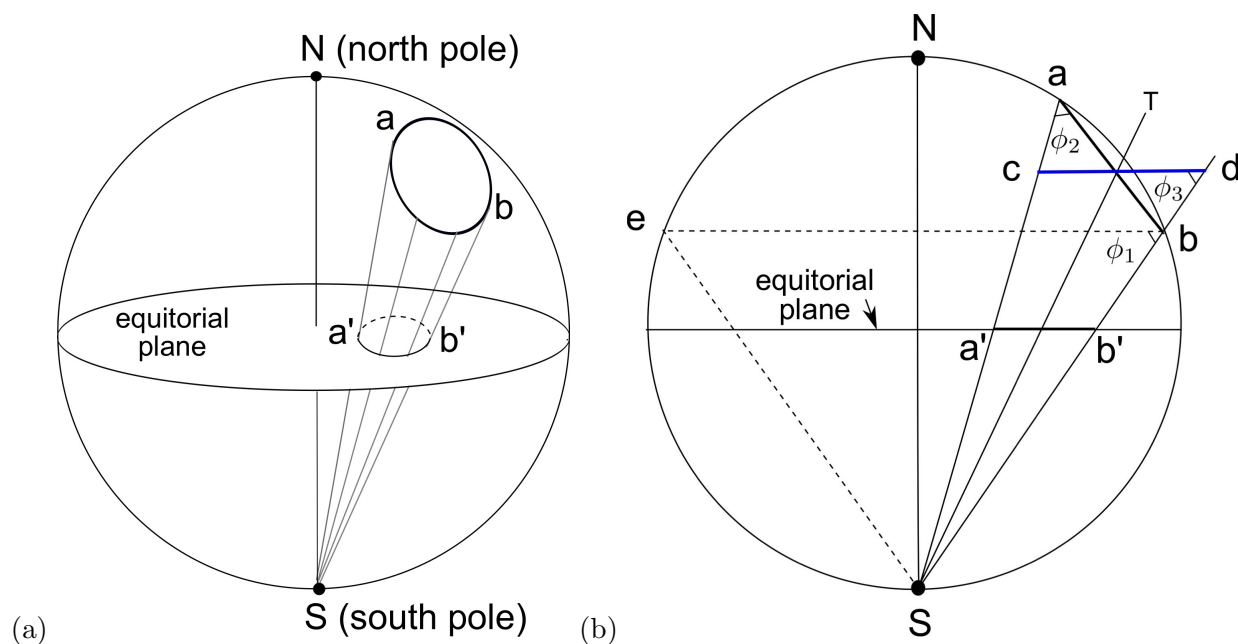


Figure 2.3: (a) Circle on the surface of a sphere projected on to the equatorial plane via the south pole. (b) Construction showing that the projection is also a circle.

This example shows that the *stereographic* projection method illustrated in Fig. 2.3 preserves angular truth; if two circles (e.g. a longitude and latitude) inscribed on the sphere cross at 90° then the projections of those two circles will also cross at that angle. We shall now consider these stereographic projections in more detail, following a brief description of why they are of importance.

2.3 Utility of stereographic projections

There is an excellent review of the history of the stereographic projection by Howarth, tracing the origin to the 2nd century BCE in the context of astronomy. Howarth describes how projections were then used in mineralogy and structural geology, where ‘the spatial orientations of a crystal face, bedding plane, fault surface etc. can be considered by imagining a plane passing through the centre of a sphere’.

Stereographic projections are two-dimensional representations which now have found numerous applications in materials science, with the method often embedded in the software that controls experimental crystallography, for example,

- the deformation of single crystals whence crystal planes rotate in order to comply with the external stress; such rotations in polycrystalline materials lead to non-random aggregates of crystals, the properties of which are in between those of single and random polycrystals. In both of these cases, it becomes necessary to define the orientations of individual crystals relative to the deformation axes, which is where stereographic projections become useful.
- When phase transformations occur in the solid state, the probability is that the product phase will form such that the atomic arrangements match as much as possible, along the parent/product interface. This often leads to a reproducible orientation relationship between the two crystals, one which can be represented on a stereographic projection in order to understand the mechanism of transformation or the deformation behaviour of the two-phase mixture. Stereographic projections can be used to decide whether the orientation relationship is reproducible or occurs by chance.
- Diffraction data can be presented on stereographic projections. It is now routine to to examine both structure and crystallographic information from polycrystalline samples on a single image, with the crystallographic data presented in the form of corresponding colours on the microstructural image and stereographic projection.

2.4 Stereographic projection: construction and characteristics

Imagine a sphere. Any plane that passes through its centre will intersect the surface of the sphere at a circle whose diameter is that of the sphere; this is known as a *great circle*, Fig. 2.4a. The primitive (great) circle is where the equatorial plane intersects the sphere Fig. 2.4b. The diameter of a great circle is the same as that of the sphere. Lines of longitude are all great circles in the spherical earth approximation.

When an intersecting plane does not pass through the centre of the sphere it results in a *small circle* at the intersection, as illustrated in Fig. 2.4c. Lines of latitude are in general small circles, the exception being the equator.

The shortest distance between two points on a sphere is along the great circle which passes through both of the points.

Fig. 2.5a shows a crystal with a cubic lattice, placed at the centre of a sphere with the $[100]$ \parallel x -axis, $[010]$ \parallel y -axis and $[001]$ \parallel z -axis of the sphere; this is the conventional orientation of the crystal in the sphere. Similarly, the orientation of an arbitrary plane can be defined by its normal, which in general is known as the *pole* of the plane. Suppose now that the normal to the (011) plane is projected so that it intersects the sphere at the point a (Fig. 2.5b), which then is projected to the

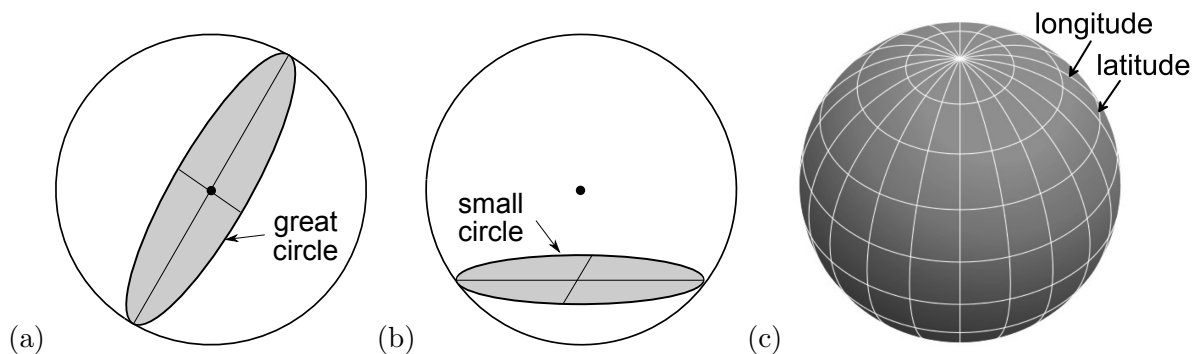


Figure 2.4: Intersections of planes with sphere. (a) Great circle inclined with respect to the north and south poles of the sphere, (b) small circle; (c) latitude and longitude lines (image courtesy of vectortemplates.com).

south pole. The intersection on the equatorial plane being the point b which represents the pole of the plane on the stereographic projection.

The plane (011) when extended so that it intersects the sphere will result in a great circle on the surface of the sphere, the trace of which can be projected on to the equatorial plane as illustrated in Fig. 2.5d. The part of the plane that is in the northern hemisphere projects as a line, and that from the southern hemisphere as a dashed-line. All points on the trace are at 90° to the pole of (011) since the pole represents the normal to the plane, another indication of how the stereographic projection maintains angular truth.

A projection of the longitudes and latitudes illustrated in Fig. 2.4c on to the equatorial plane would lead to a net, known as the 'Wulff net' in which the resulting great circles are spaced at equal angles as illustrated in Fig. 2.6 where the angular intervals are 2° . The net can be used to measure angles between two poles on a stereographic projection by rotating the net such that both poles lie on the same great circle, followed by counting the degrees separating them. Note that the angle between two great circles will be the same as the angle between their poles.

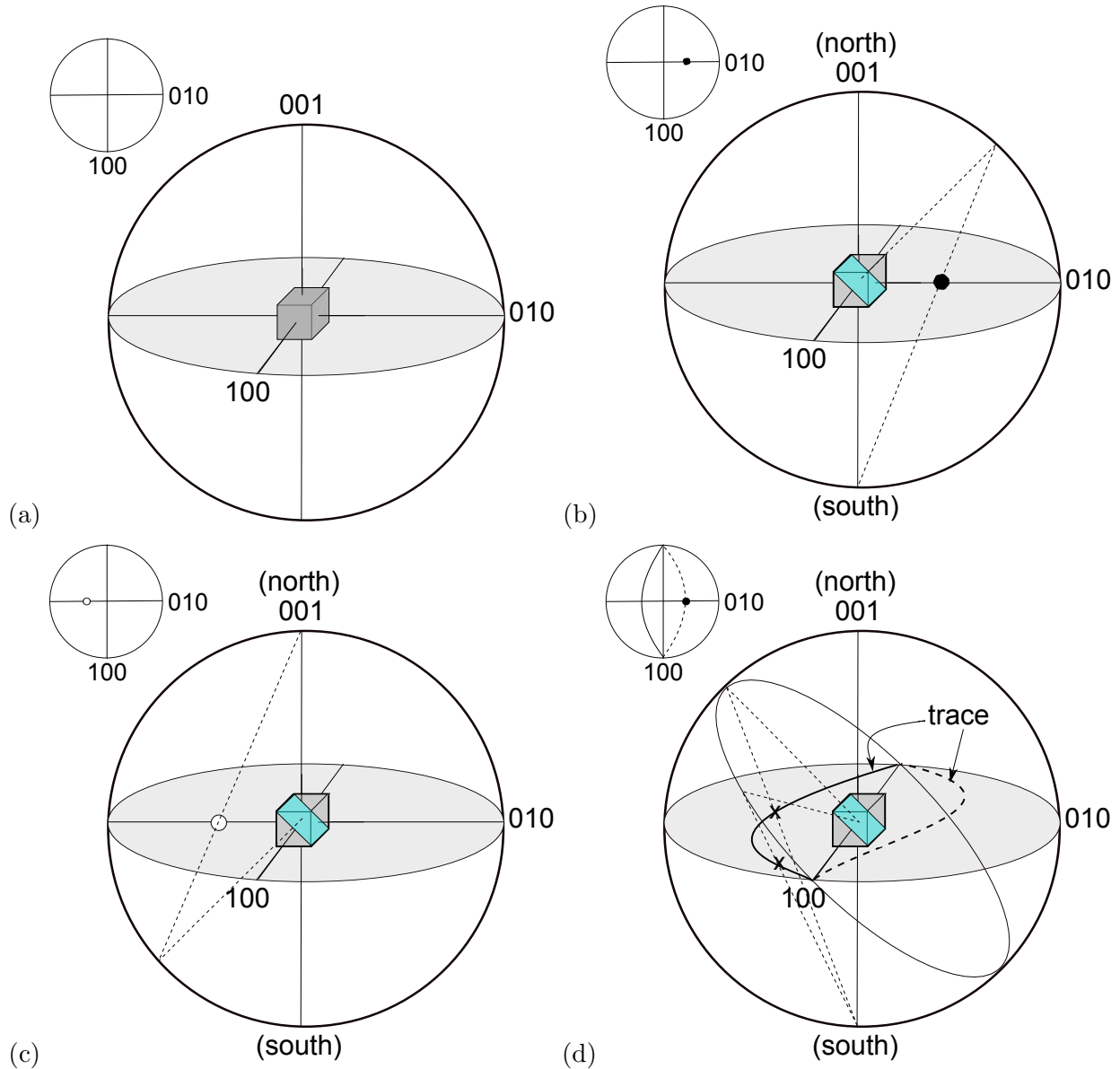


Figure 2.5: Plotting plane normals on a stereographic projection. The insets, top-left in each case, show a plan view of the equatorial plane. (a) Crystal places at the centre of the sphere. (b) Projection of the pole of (011). (c) Projection of (011). (d) Projection of the trace of the great circle which is (011) on to the equatorial plane. The trace of the plane in the southern hemisphere is marked as a dashed curve. The crosses identify the intersections of the projection lines with the equatorial plane.

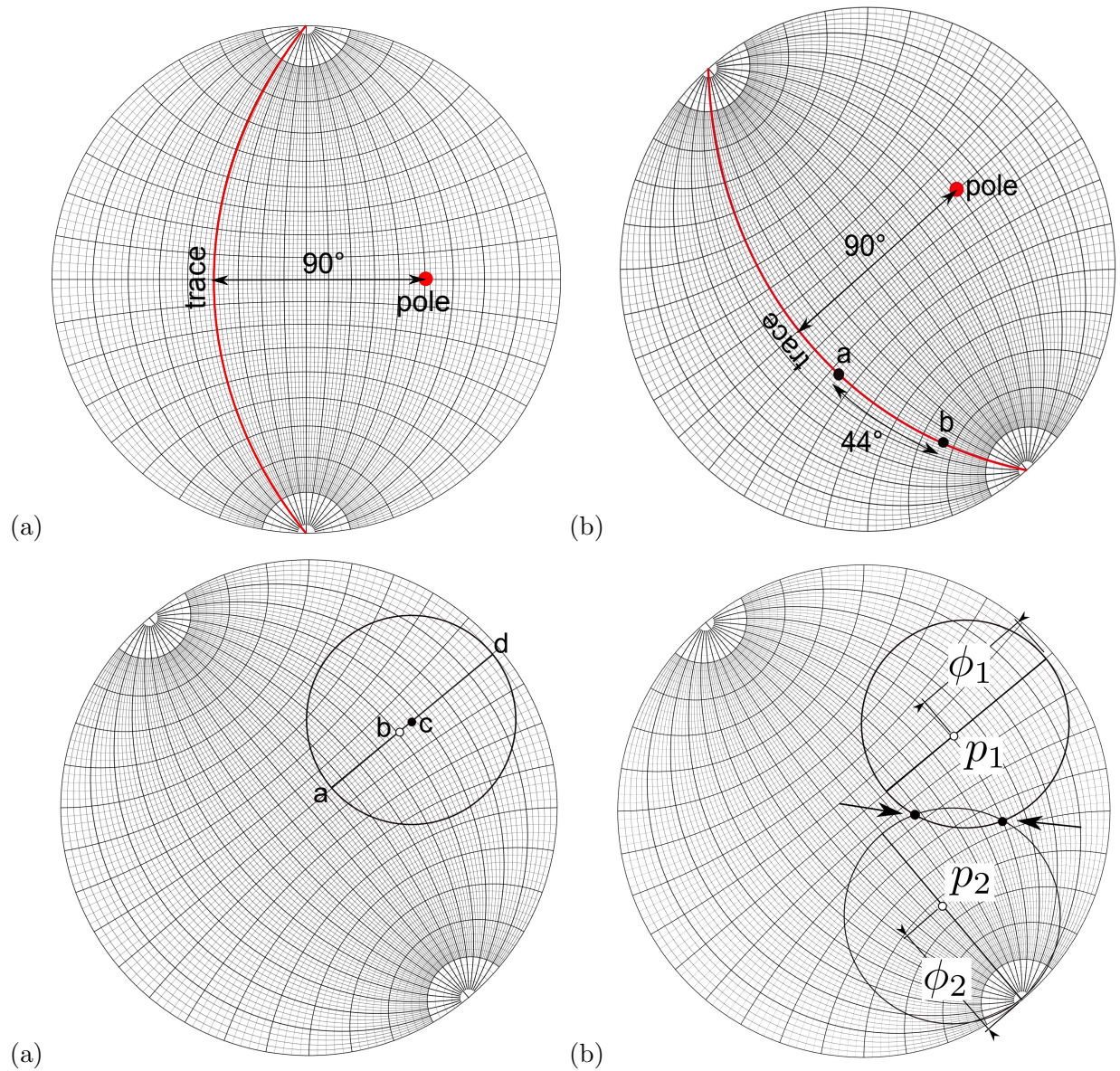


Figure 2.6: The Wulff net. (a) Relation between pole and trace of a plane. (b) The net is rotated until the poles *a* and *b* lie on the same great circle to measure the angle in between. (c) The geometrical centre *c* of the small circle is different from its angular centre *b*. The angles *ab* and *bd* as measured on the great circle are identical. The distances *ac* and *cd* are identical when measured on a ruler. (d) The poles identified with arrows are both located at angles ϕ_1 to p_1 and ϕ_2 to p_2 .

The curve representing a great circle on a Wulff net is itself an arc of a circle, a result which follows from the fact that the projection method preserves angular truth. This arc is from a circle that in general has a radius r greater than that of the net (r_o). We now derive the relationship between r , r_o and the offset x of the trace of the great circle from the origin.

Referring to the figure below, the distance ab is $2r_o$; the Pythagoras theorem then gives

$$r^2 - r_o^2 = (r - x)^2$$

so it follows that $r = (x^2 + r_o^2)/2x$ with $r_o \leq r \leq \infty$.

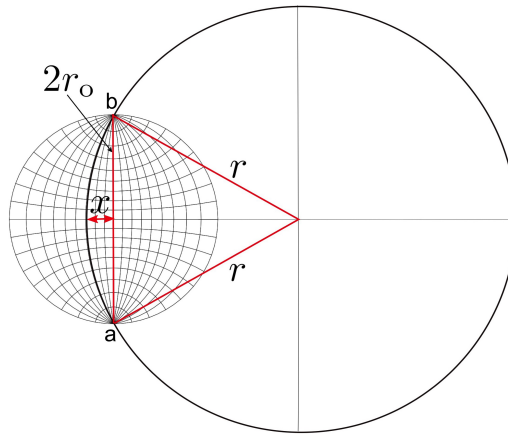


Fig. 2.7a,b show the stereographic projection for the cubic system, with the rotational symmetry elements related to the crystallographic directions about which the rotations occur. Fig. 2.7c shows the stereographic projection being used to show how the elastic modulus of a single crystal of ferritic iron varies between 131 and 284 GPa as a function of the crystallographic orientation, in a manner consistent with its crystalline symmetry. Even aggregates of crystals often do not show collective macroscopic-properties that are isotropic because the crystals are not distributed at random. Polycrystalline ferritic steel sheet in which the crystals are aligned with the $\langle 001 \rangle$ direction and with the $\{110\}$ planes aligned to the rolling plane, exhibit modulus variation in the range 140 to 210 GPa. The level of anisotropy in aggregates can be controlled, as we shall see in later chapters, to suit specific purposes such as the formability of metal sheets or the magnetic properties of transformer steels.

2.5 Stereographic representation of point groups

We shall now show using sketch stereograms, that the operation of a diad followed by an inversion (i.e. $\bar{2}$) is equivalent to a mirror plane. Do the operations $\bar{3}$ and $\bar{6}$ lead to centres of symmetry?

A general pole on a stereographic projection is one that is not located at particular symmetry elements such as the rotation axis or on a mirror plane. The black dot on Fig. 2.8a is a general

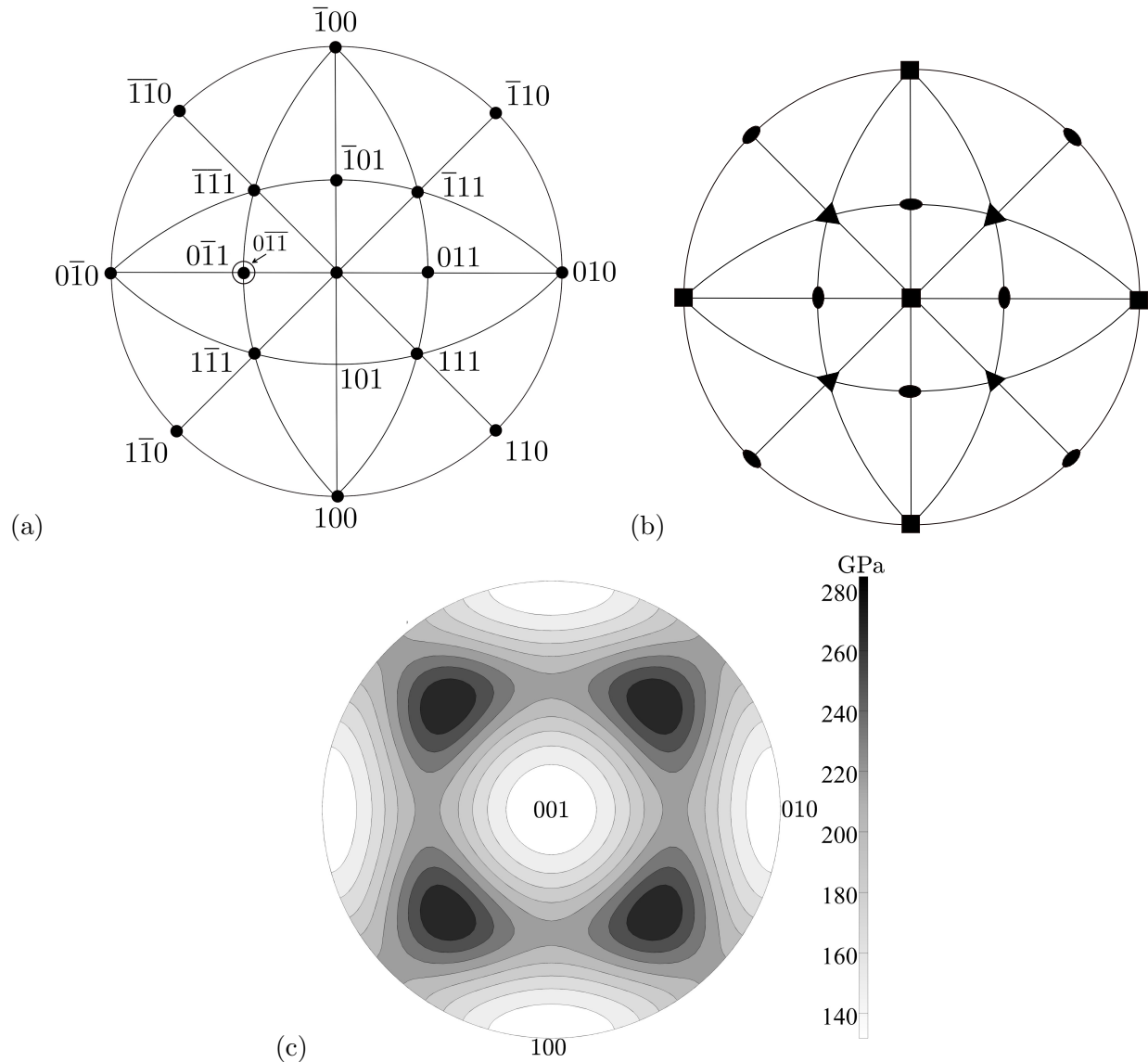


Figure 2.7: Stereographic projections for the cubic system. (a) Showing the standard way of drawing the projection with the locations of $[100]$ and $[010]$ on the perimeter and $[001]$ at the centre. (b) The symmetry elements. The filled squares are tetrads, the ellipses are diads and triangles are triads. The tetrads are at $\langle 001 \rangle$, triads at $\langle 111 \rangle$ and diads at $\langle 011 \rangle$. Anything with cubic symmetry must have four triads. (c) Variation in the elastic modulus of a single crystal of bcc iron as a function of orientation. Diagram courtesy of Shaumik Lenka, constructed using data from Dieter (1988).

pole which on the operation of a diad results in a second pole as shown in Fig. 2.8b. When inverted through the centre, this second pole intersects the stereographic sphere in the southern hemisphere and hence is shown as an open circle in Fig. 2.8c, which shows that the net operation of a diad followed by an inversion is a mirror plane parallel to the plane of the diagram. It is seen that $\bar{2} \equiv m$.

The operation of a triad on a general pole leads to three such poles, which after inversion result in the situation illustrated in Fig. 2.8e, which shows that the point group $\bar{3}$ belongs to a class that have centres of symmetry whereas $\bar{2}$ and $\bar{6}$ do not.

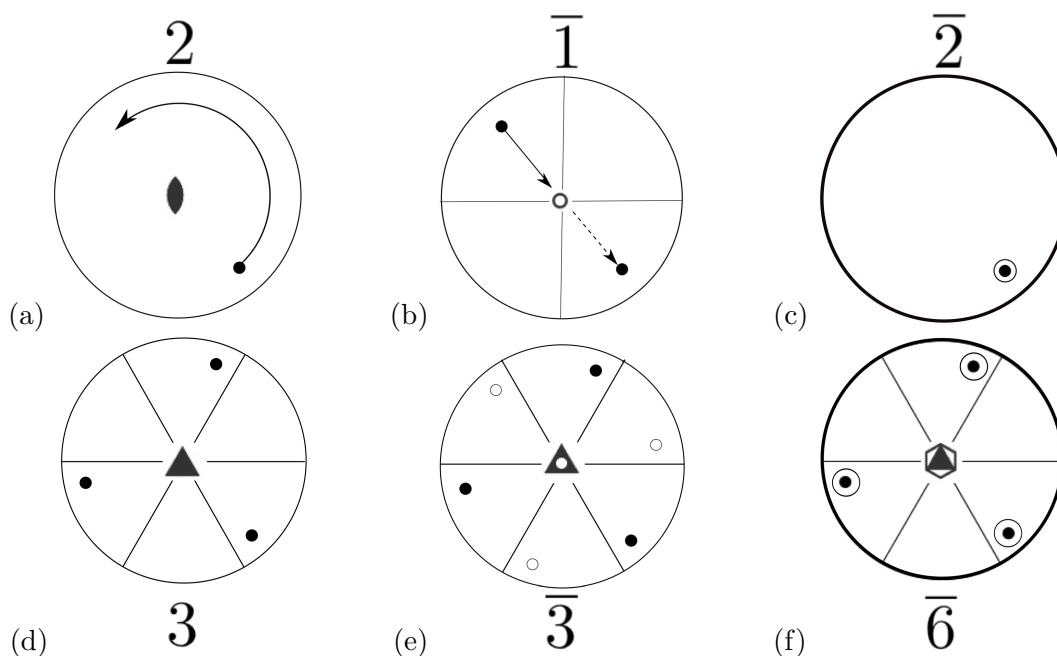


Figure 2.8: (a) An arbitrary pole is rotated by 180° about the diad normal to the plane of the diagram, to generate the second pole illustrated in (b). This second pole is inverted through the centre to lead to the result in (c) to represent the full operation of the inversion diad $\bar{2}$. (d) Triad, (e) inversion triad and (f) inversion hexad. Mirror planes in (c) and (f) are identified using bold circles.

2.6 The point groups $3m$ and $m\bar{3}$

Referring to Table 1.2, we now explain using sketch stereograms, the difference between the point groups $3m$ and $m\bar{3}$.

According to the conventions described on page 17, the point group $3m$ implies that there is a single triad with the secondary axis being the normal of the mirror plane. The triad ensures that there would be three such mirror planes. There is no mirror plane normal to the triad (Fig. 2.9a),

which means that the atomic arrangement along one end of the triad is different from the opposite end. Such a crystal may display spontaneous polarisation and the point group $3m$ is said to be a *polar point group*, which include 1 (triclinic); 2, m (monoclinic); $mm2$ (orthorhombic); 4, $4mm$ (tetragonal); 3, $3m$ (trigonal); 6, $6mm$ (hexagonal). There are no polar groups in cubic crystals. Gallium nitride as a polar material ($6mm$) is of huge interest in the manufacture of light emitting diodes – Fig. 2.9b shows that the top surface normal to the hexad is different from the bottom surface. During deposition of GaN films on substrates, the layers deposit predominantly with uniform polarity except some regions which have opposite polarity and are regarded as defects that lead to poor control of electrical properties.

The point group $m3$ belongs to the cubic crystal class with the first symbol m parallel to the z axis (page 17) and the mandatory symbol ‘3’ to follow since the defining symmetry of a cubic system is four triads, in this case inversion triads. It is evident from the plotting of a general pole and its symmetry related poles shown in Fig. 2.9c that there is a centre of symmetry. Pyrite belongs to the cubic class with point group $m3$. Fig. 2.9d shows a projection of the crystal structure of pyrite, which is primitive cubic. The structure can be compared with the stereogram showing the point group symmetry in Fig. 2.9c. Bearing in mind that point groups do not include translations, the glide planes and screw axes indicated in Fig. 2.9d become mirrors and diads respectively.

Crystals which lack a centre of symmetry can be piezoelectric, i.e. they develop a dipole on being deformed and will change shape on the application of an electrical field. Under normal conditions the crystal has positive and negative electrical charges which are symmetrically distributed, leaving the crystal in a neutral state when homogeneously deformed. The application of a stress causes charge asymmetry, and the development of a voltage across the crystal. PbTiO_3 is such a substance (Fig. 2.10) where for example, the titanium atom is not located at exactly $\frac{1}{2}, \frac{1}{2}, \frac{1}{2}$. The structure is primitive tetragonal, with point group $4mm$.¹

The stereogram illustrated in Fig. 2.10b shows that the structure has no centre of symmetry. Secondly, if an atom is placed at a general position (marked a) then there will be seven other identical atoms in the unit cell, inconsistent with the structure illustrated in Fig. 2.10a. An atom placed on a tetrad (marked c) will generate just one atom per unit cell; thus, there is just one Ti at $\frac{1}{2}, \frac{1}{2}, 0.572$. The oxygens at $\frac{1}{2}, \frac{1}{2}, 0$ and $\frac{1}{2}, \frac{1}{2}, 1$ also lie on a tetrad, and since they are shared between two cells, there is only one such oxygen in the unit cell. An atom, such as the oxygen at $0, \frac{1}{2}, \frac{1}{2}$, placed on the mirror plane as illustrated by the poles marked b , would generate two such atoms in the cell (the four on the vertical faces are each shared by two cells).

This example shows how the placing of an atom within a unit cell must be consistent with the symmetry elements of the cell because there must be identical atoms at all symmetry related positions.

There are many other consequences of whether or not a crystal has a centre of symmetry. The free energy of a small volume element containing a one-dimensional composition gradient varies as

¹i.e. by the convention quoted on page 17, the z direction is assigned to the four-fold rotation axis followed by m for the mirrors with normals parallel to the x and y axes, and the final symbol for the tertiary mirrors with normals between the x and y axes.

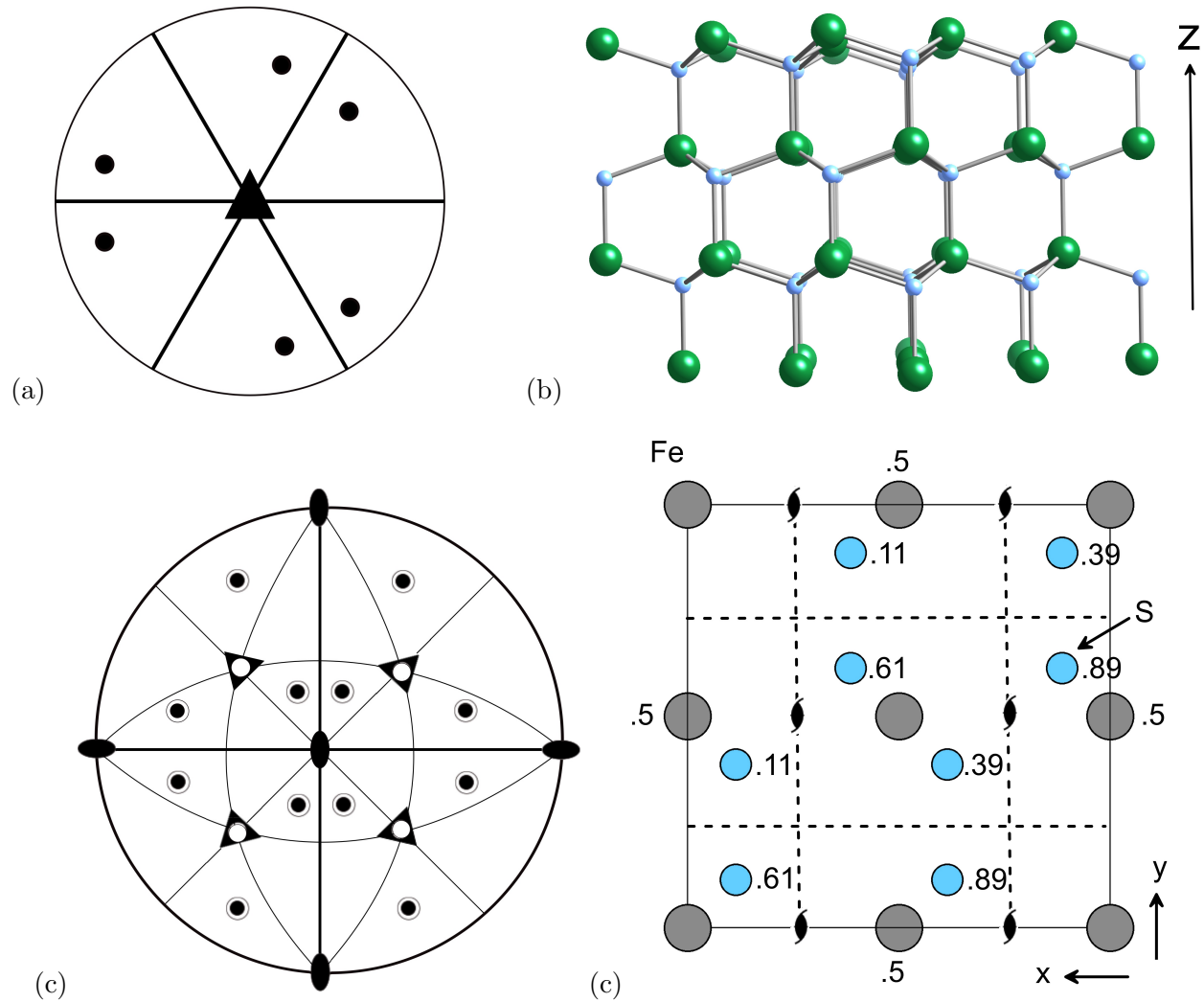


Figure 2.9: Sketch stereograms showing what happens to a general pole on the operation of the following point groups (bold lines represent mirror planes): (a) trigonal $3m$. (b) The structure of GaN with point group symmetry $6mm$, viewed with the 6-fold axis along z . The gallium atoms are labelled green. (c) Cubic $m\bar{3}$. (d) Projection of the unit cell of pyrite (FeS_2) with the fractional z coordinates indicated, glide planes marked with dashed lines and screw diads. Not all the symmetry elements are illustrated for simplicity.

follows:

$$g = g\{\bar{c}\} + \kappa_1 \frac{dc}{dz} + \kappa_2 \frac{d^2c}{dz^2} + \kappa_3 \left(\frac{dc}{dz}\right)^2 \quad (2.1)$$

where c is the concentration, $g\{\bar{c}\}$ is the free energy of a homogeneous solution with composition \bar{c} , z is the distance and κ_i are specific functions of the dependence of free energy on the gradients of concentration as described elsewhere. In this, κ_1 is zero for a centrosymmetric crystal since the free energy must then be invariant to a change in the sign of the coordinate z .

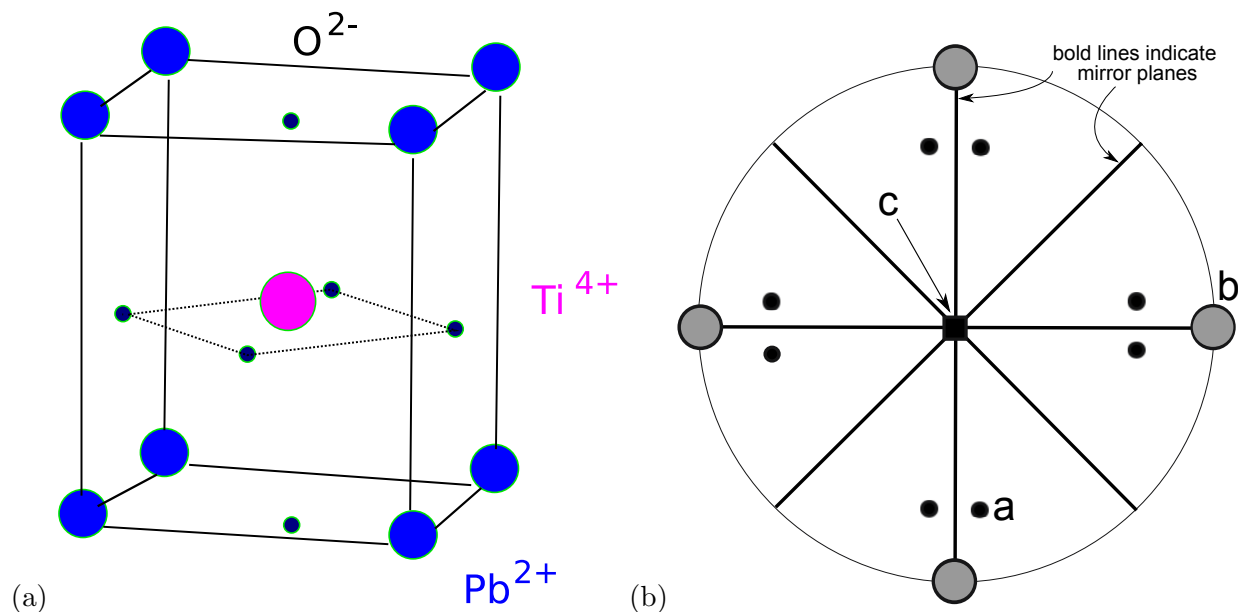


Figure 2.10: (a) Lead titanate (PbTiO₃) is tetragonal with $a = 0.3904$ nm and $c = 0.4152$ nm. The Pb is located at coordinates $(0,0,0.116)$, the Ti at $(\frac{1}{2}, \frac{1}{2}, 0.572)$, an oxygen atom at $(0, \frac{1}{2}, \frac{1}{2})$ and another oxygen at $(\frac{1}{2}, \frac{1}{2}, 0)$. The structure is primitive tetragonal with point group $4mm$. (b) Stereogram showing the symmetry operations associated with the point group $4mm$.

2.7 Summary

A circle on a sphere projects as a circle on the stereographic projection; angular relationships are therefore preserved. The method is therefore well suited to look at angles between planes or directions in a crystal. The symmetry of the crystal in its three dimensions becomes easy to visualise by plotting the symmetry elements in their correct angular orientations on a stereographic projection. The placing of atoms inside the unit cell during attempts to solve structure must clearly be consistent with the symmetry determined, for example, from the external form of well-formed crystals.

The stereographic projection can also be used quantitatively, by superimposing a Wulff net to directly measure angles between a pair of poles. The net consists of projections of great and small circles, rather like the longitudes and latitudes on a globe representing the earth. The shortest distance between two points on the surface of a sphere is when the two points are located on an arc of a circle which has the same diameter as the sphere. When using a Wulff net to measure the angle, it therefore is necessary to locate the two poles on a great circle.

We have seen that some quite elementary considerations of symmetry can indicate the occurrence of phenomena such as piezoelectricity, or polar materials. There is much more to be explored in the chapters that follow.

Chapter 3

Stereograms for Low Symmetry Systems

3.1 Introduction

In the cubic system, a plane normal (pole) with indices hkl is parallel to a direction uvw when $h = u$, $k = v$, $l = w$; thus the normal to (123) is parallel to $[123]$. This is not generally the case for less symmetrical systems. Fig. 3.1 illustrates this for a two-dimensional unit cell in which $b > a$.

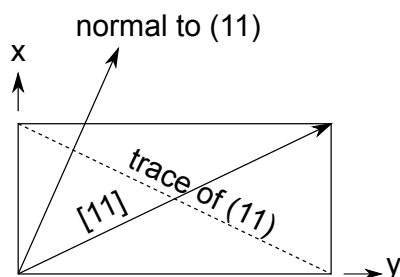


Figure 3.1: The direction $[11]$ is not parallel to the normal to the plane (11) . On the other hand, the directions parallel to the cell edges, *i.e.* $[01]$ and $[10]$ are parallel to the normals of (01) and (10) respectively.

The principles for the plotting of poles on stereographic projections are nevertheless identical for any lattice. However, the cubic system exhibits extraordinary symmetry so angular relationships on the stereographic projection are not dependent on the lattice parameter. This is not the case for other lattices with lesser symmetry, the stereograms of which will not only appear different from a distance, but for the same lattice type, the angular positions become dependent on the lattice parameters. Fig. 3.2a,b shows how the projections differ in the case of the cubic and orthorhombic lattices where the absence of tetrads in the latter is obvious. Fig. 3.2c shows how the projection changes when one of the lattice parameters of the orthorhombic lattice is changed relative to that illustrated in Fig. 3.2b.

The fact that directions are not in general parallel to plane normals with the same indices is apparent from a comparison of Fig. 3.2c,d.

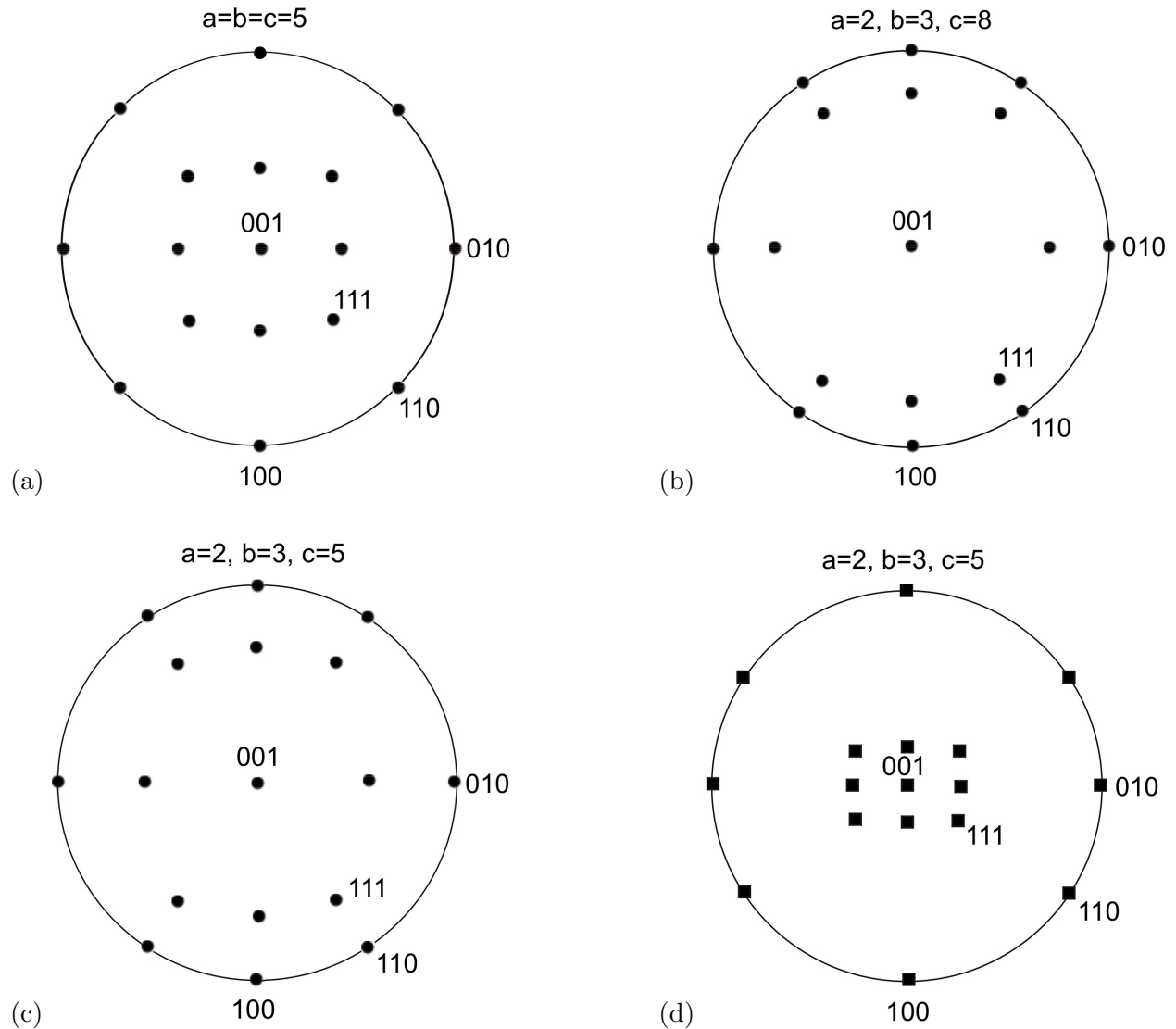


Figure 3.2: Stereographic projections centred on the 001 pole. (a) Cubic, lattice parameter 5 units. (b) Orthorhombic, lattice parameters 2, 3, 8 units. (c) Orthorhombic, lattice parameters 2, 3, 5 units. (d) The orthorhombic cell as in (c) but with directions plotted instead of poles.

3.2 Hexagonal System

The unit cell has $a = b \neq c$ and $\alpha = \beta = 90^\circ$ with $\gamma = 120^\circ$. The normals to the (100) and (010) planes therefore make an angle of 60° (Fig. 3.3a). This is shown on the projection in Fig. 3.3, which highlights a special difficulty with the hexagonal system.

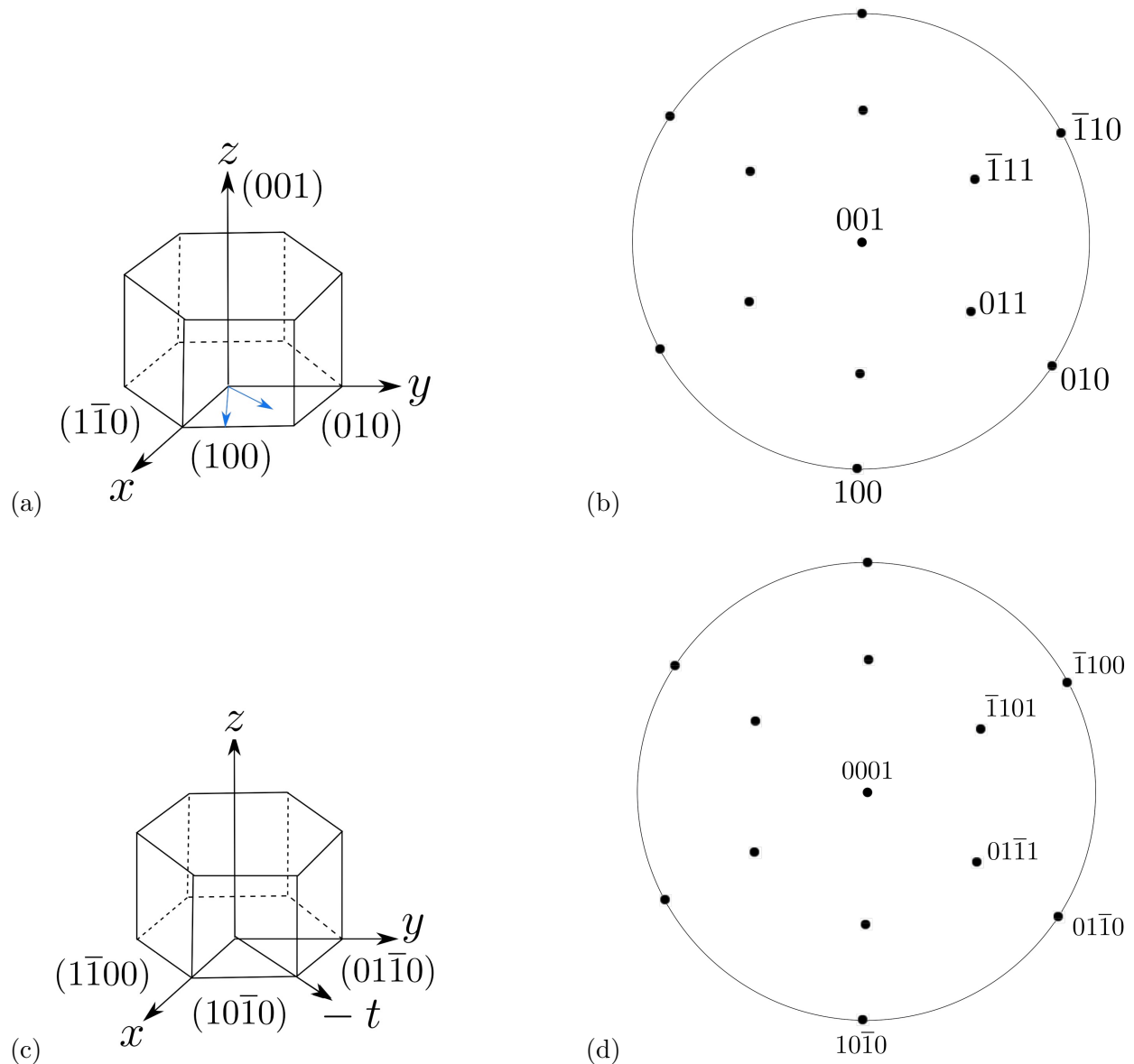


Figure 3.3: (a) Showing the hexagonal cell with the normals to the (100) and (010) planes identified with coloured arrows. (b) Stereographic projection of hexagonal structure (lattice parameters $a = 2$, $b = 2$ and $c = 3$ units with $\gamma = 120^\circ$) centred on the 001 pole. (c) Showing the hexagonal cell, now in four index notation. (d) Corresponding stereogram in four index notation.

It is evident from Fig. 3.3a that the (100), (010) and ($\bar{1}10$) are planes belonging to the same form {100}, *i.e.*, they are crystallographically equivalent. And yet, they have different indices. To eliminate this discrepancy, a four index system is frequently used for hexagonal lattices by introducing a fourth axis (labelled d in Fig. 3.3c), which gives plane indices as $hkil$, where from geometry, $i = -(h + k)$. This has the effect of giving equivalent planes the same combination of digits in their indices. Thus, (100), (010) and ($\bar{1}10$) become ($10\bar{1}0$), ($01\bar{1}0$) and ($\bar{1}100$) respectively.

A similar conversion for directions from uvw to $UVJW$ is a little more difficult because it is designed in such a way that $J = -(U + V)$ and at the same time, the Weiss zone law in which a plane hkl containing a direction uvw is satisfied

$$hu + kv + lw = 0 \quad (3.1)$$

so that

$$hU + kV + iJ + lW \quad \text{should equal zero.}$$

On substituting for $i = -(h + k)$ we get,

$$\begin{aligned} hU + kV + (-h - k)J + lW &= 0 \\ h(U - J) + k(V - J) + lW &= 0 \end{aligned} \quad (3.2)$$

On comparing the coefficients of h , k and l , and noting that $J = -(U + V)$,

$$\begin{aligned} U - J = u & \quad u = 2U + V & \quad U = \frac{1}{3}(2u - v) \\ V - J = v & \rightarrow v = U + 2V & \quad \text{and} \quad V = \frac{1}{3}(2v - u) \\ W = w & \quad w = W & \quad J = -\frac{1}{3}(u + v) \end{aligned} \quad (3.3)$$

Table 3.1: Directions of the same form now have similar combinations of digits in the four figure notation.

Three-index notation	Four-index notation
[100]	$\frac{1}{3}[2\bar{1}\bar{1}0]$
[010]	$\frac{1}{3}[\bar{1}2\bar{1}0]$
[110]	$\frac{1}{3}[11\bar{2}0]$
[uvw]	$\frac{1}{3}[2u - v, 2v - u, -(u + v), 3w]$

Iron, by far the most used metallic material in the world, under ambient conditions is cubic-I with one iron atom located at each lattice point. The common slip system is $\{0\bar{1}1\}\langle 111 \rangle$, each containing

two independent slip directions of the form $\langle 111 \rangle$. There are therefore, twelve independent slip systems, making the iron ductile in polycrystalline form. The same can be demonstrated for the cubic-I form of iron. This makes iron very ductile.

The cubic-I form of iron is stabilised under ambient conditions by its ferromagnetic properties; ruthenium and osmium, which in terms of outer electronic structure are iron analogues in the periodic table, do not exhibit ferromagnetism and hence have hexagonal crystal structures. In the absence of its ferromagnetic properties, the stable form would be hexagonal with a motif of a pair of identical Fe-atoms, one at 0,0,0 and another at $\frac{1}{3}, \frac{2}{3}, \frac{1}{2}$. The easy-slip system is then $\{0001\}\langle 11\bar{2}0 \rangle$. Since there is only one (0001) plane in which there are three directions of the form $\langle 11\bar{2}0 \rangle$, polycrystalline hexagonal iron is relatively brittle since the number of slip systems in each crystal is less than the required five. So in the absence of ferromagnetism, we would not have civilisation in the form that we know today.

There are caveats to this story. Deformation can occur by mechanisms other than slip, for example, mechanical twinning, so that the five independent slip system requirement is not sufficient to determine the ductility of a polycrystalline material. And iron below its Curie temperature is not strictly cubic, but tetragonal because the magnetic spins in any given crystal tend to be aligned along a $\langle 100 \rangle$ axis. However, the tetragonality is quite small and can be neglected in most experiments, although it does manifest on a macroscopic scale via the magnetostrictive effect, which is the variation in the length of a sample subjected to a magnetic field.

3.3 Summary

Complications arise once the defining symmetry of the cube, i.e., four triads, is lost. Directions and plane normals with the same indices are then not necessarily parallel and hence have to be distinguished on a stereographic projection. Furthermore, the extent of the discrepancy relative to the cubic system depends on the anisotropy of the lattice parameters and the angles between the basis vectors of the system concerned.

The hexagonal system poses a particular problem of communication because of the nature of the special symmetry of the hexad. For example, the crystallographically equivalent planes (100), (010) and ($1\bar{1}0$) have indices that are not permutations of the same set of digits. The Miller-Bravais four-index system eliminates this ambiguity but requires additional work to ensure that the Weiss zone rule is satisfied. Whether the intellectual cost of the four-index system over the usual three-index notation is justified by its elegance is a matter of taste.

Chapter 4

Space Groups

4.1 Introduction

A point group is a collection of symmetry elements passing through a point, and therefore, necessarily does not include translations. *Space groups*, in contrast, include translations that are fractions of a repeat unit, for example, a 2_1 axis which involves a rotation of 180° followed by a translation of $\frac{1}{2}$ of the repeat distance along the axis. Glide planes involve reflections followed by fractional translations. These translations are small, and hence do not manifest when the point group is determined from the external shape of well-formed crystals. However, they have consequences in structure determination and on other properties of crystals. There are 230 space groups which are made from combinations of the 32 crystallographic point groups with the 14 Bravais lattices.

The relationships between the placing of atoms in the unit cell and the symmetry of the structure of lead titanate was described on page 29. The structure of PbTiO_3 is primitive tetragonal with point group $4mm$. Since there are no screw axes or glide planes, the space group symbol for the titanate is $P4mm$, where the first symbol is to identify the lattice type as primitive. In this chapter, we will consider a case where translational symmetry elements¹ are present.

4.2 Screw axes and glide planes

A proper rotation axis designated N brings a motif into coincidence after a rotation of $\frac{2\pi}{N}$. A screw axis, designated N_p , does the same but only when a translation of $\frac{p}{N} \times t$ follows the rotation by $\frac{2\pi}{N}$. Here t is the distance between lattice points parallel to the axis. A screw diad (2_1) is illustrated in Fig. 4.1, involving a rotation of 180° followed by a translation of $\frac{1}{2}t$ parallel to the axis. Other

¹other than the normal periodicity of a lattice

rotation axes following the same logic in terms of notation are: 3_1 , 3_2 , 4_1 , 4_2 , 4_3 , 6_1 , 6_2 , 6_3 , 6_4 and 6_5 .

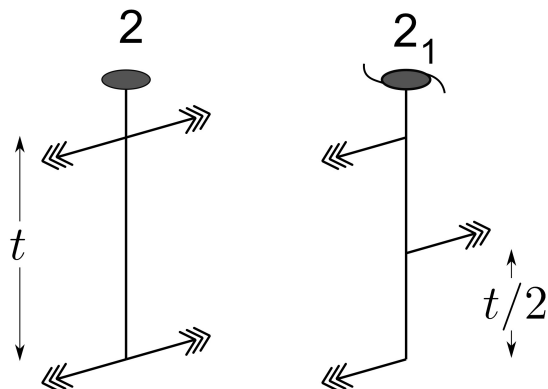


Figure 4.1: An illustration of the operation of a diad where the structure is restored by a rotation of 180° , and a screw diad which involves the same rotation but then a translation along the axis by 0.5 (hence the notation 2_1) of the repeat distance t .

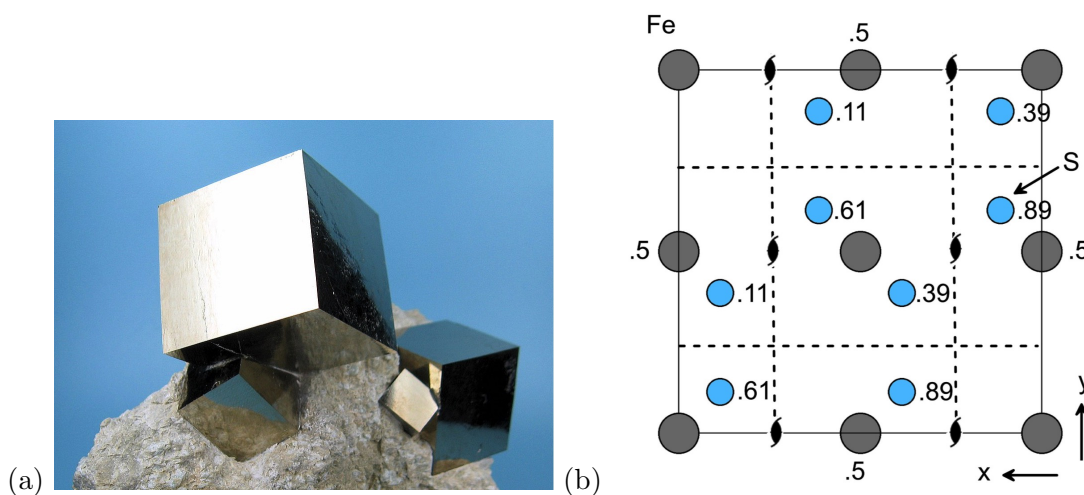
Glide planes are like mirror planes but a reflection is followed by a translation in order to recover the symmetry. The terminology for glide planes is explained in Table 4.1; the translations following reflection are parallel to the glide plane, the exception being the diamond glide in a body-centred cubic structure.

Table 4.1: Symbols for glide planes. ‘f.c.c.’ and ‘b.c.c.’ are abbreviations for face-centred cubic and body-centred cubic respectively.

Glide character	Direction	Magnitude	Symbol
Axial glide	parallel to a , b or c axis	$\frac{1}{2}(a, b, \text{ or } c)$	$a, b, \text{ or } c$
Diagonal glide	parallel to face diagonal	$\frac{1}{2}(a + c), \frac{1}{2}(b + c)$ or $\frac{1}{2}(a + b)$	n
Diamond glide (f.c.c.)	parallel to face diagonal	$\frac{1}{4}(a + c), \frac{1}{4}(b + c)$ or $\frac{1}{4}(a + b)$	d
Diamond glide (b.c.c.)	parallel to body diagonal	$\frac{1}{4}(a + b + c)$	d

4.3 Pyrite

Pyrite is an iron sulphide, often known as *fools gold* because it has a gold-like colour. It crystallises as clusters of perfectly formed cubes (Fig. 4.2); therefore the external shape indicates that it belongs to the cubic crystal class with four triads along the body diagonals as the defining symmetry. The crystal structure illustrated has a primitive cubic lattice with a motif of four iron atoms and eight sulphur atoms per lattice point. There are 2_1 screw diads that involve a rotation of 180° and a translation by a fraction $\frac{1}{2}$ of the repeat distance along the screw axis. In addition, there are glide planes parallel to the cube faces, involving a reflection and then a translations by $\frac{1}{2}$ the repeat distance parallel to the cube edges. They therefore are a -glide planes. There also is a centre of symmetry at the body-centre of the cube $(\frac{1}{2}, \frac{1}{2}, \frac{1}{2})$ and $(0,0,0)$, so the triads are in fact $\bar{3}$ inversion triads.



Wyckoff Positions of Group $Pa\bar{3}$ (No. 205)

Multiplicity	Site symmetry	Coordinates
24	1	(x,y,z) $(-x+1/2,-y,z+1/2)$ $(-x,y+1/2,-z+1/2)$ $(x+1/2,-y+1/2,-z)$ (z,x,y) $(z+1/2,-x+1/2,-y)$ $(-z+1/2,-x,y+1/2)$ $(-z,x+1/2,-y+1/2)$ (y,z,x) $(-y,z+1/2,-x+1/2)$ $(y+1/2,-z+1/2,-x)$ $(-y+1/2,-z,x+1/2)$ $(-x,-y,-z)$ $(x+1/2,y,-z+1/2)$ $(x,-y+1/2,z+1/2)$ $(-x+1/2,y+1/2,z)$ $(-z,-x,-y)$ $(-z+1/2,x+1/2,y)$ $(z+1/2,x,-y+1/2)$ $(z,-x+1/2,y+1/2)$ $(-y,-z,-x)$ $(y,-z+1/2,x+1/2)$ $(-y+1/2,z+1/2,x)$ $(y+1/2,z,-x+1/2)$
8	.3.	(x,x,x) $(-x+1/2,-x,x+1/2)$ $(-x,x+1/2,-x+1/2)$ $(x+1/2,-x+1/2,-x)$ $(-x,-x,-x)$ $(x+1/2,x,-x+1/2)$ $(x,-x+1/2,x+1/2)$ $(-x+1/2,x+1/2,x)$
4	-.3.	$(1/2,1/2,1/2)$ $(0,1/2,0)$ $(1/2,0,0)$ $(0,0,1/2)$
4	-.3.	$(0,0,0)$ $(1/2,0,1/2)$ $(0,1/2,1/2)$ $(1/2,1/2,0)$

Figure 4.2: (a) Naturally occurring pyrite (FeS_2). Micrograph due to Charles Millan, Wikimedia, under license CC BY-SA 3.0. (b) The crystal structure of pyrite projected on to the $\{001\}$ plane. (c) Wyckoff table for space group $Pa\bar{3}$, courtesy of the Bilbao crystallographic server.

It is important to note that these small translations associated with the glide plane and screw axis

do not manifest on the macroscopic shape of the crystal, so they appear as if they are mirror planes and diads, respectively. Therefore, the point group is $m\bar{3}$. This point group does not describe the atomic arrangement inside the crystal so we need to use instead the space group, which would be $Pa\bar{3}$.

Since there is a centre of symmetry at each iron atom, and a triad passing through each iron atom, the site symmetry of each iron atom is $\bar{3}$. A triad also passes through each sulphur atom but there is no centre of symmetry there, so the site symmetry at each sulphur atom is 3. The Wyckoff table for the space group confirms therefore that there should be four iron atoms and eight sulphur atoms in the unit cell.

4.4 Cementite

Cementite is a compound of iron with an approximate chemical composition Fe_3C . It has an orthorhombic lattice with parameters $a = 0.50837$ nm, $b = 0.67475$ nm and $c = 0.45165$ nm. There are twelve atoms of iron in the primitive unit cell and four of carbon, as illustrated in Fig. 4.3.

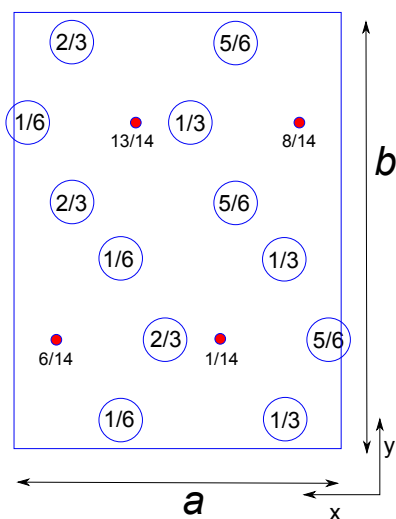


Figure 4.3: Crystal structure of cementite projected on to the (001) plane. The large atoms are iron and the red ones carbon.

The lattice type is primitive (P). Referring to Fig. 4.4, there are n -glide planes normal to the x -axis, at $\frac{1}{4}x$ and $\frac{3}{4}x$ involving translations of $\frac{b}{2} + \frac{c}{2}$. There are mirror planes normal to the y -axis and a -glide planes normal to the z -axis, at heights $\frac{1}{4}z$ and $\frac{3}{4}z$ with fractional translations of $\frac{a}{2}$ parallel to the x -axis. Following the convention in Fig. 1.11a, the space group symbol is therefore $Pnma$.

Notice from the Wyckoff table and Fig. 4.4b, that the site symmetries for the iron atoms are of two kinds. Four of the iron atoms lie on mirror planes and eight are at general positions. Similarly, we expect four carbon atoms in the cell because their site symmetries are mirrors.

The structure of cementite clearly is very anisotropic so its properties, such as the elastic moduli, also vary strongly with the direction within the crystal. The shear modulus C_{44} is exceptionally small, some two times smaller than the corresponding term for aluminium. Nevertheless, the cementite has an exceptionally large ideal shear strength because *elastic* deformation reduces its symmetry from orthorhombic to monoclinic (space group $P2_1/c$), with an accompanying increase in three dimensional covalent bonding that stiffens the material.

In the context of plastic deformation, the slip systems on which dislocation glide has been observed include $(001)[100]$, $(100)[010]$, $(100)[001]$, $(010)[001]$ and $(010)[100]$ but the complex arrangement of atoms means that slip is actually quite difficult to achieve, making the cementite very hard. There may be other slip systems that operate when the cementite is forced to deform in a phase mixture such as pearlite, but the Burgers vectors of slip dislocations would nevertheless be large when compared with dislocations in the allotropic forms of iron.

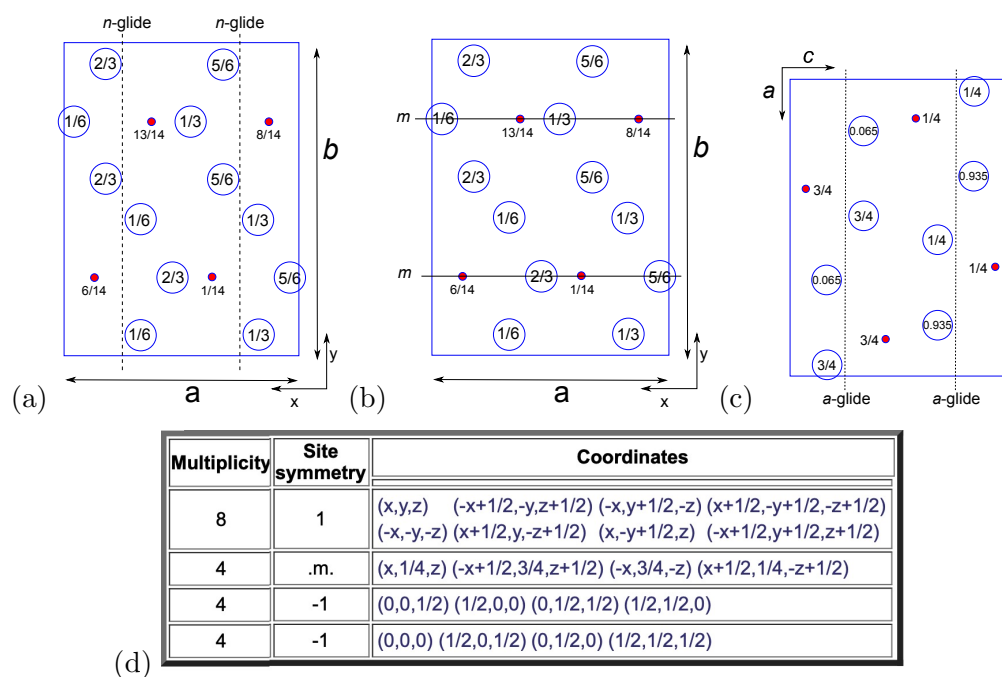


Figure 4.4: Symmetry elements in the cementite structure. (a) n -glide planes. (b) Mirror planes. (c) a -glide planes (four pairs of iron atoms share the same coordinates along x and z , so there appear to be only eight Fe atoms in the cell. The overlapping coordinates are omitted for simplicity).

4.5 Shape of Precipitates

Crystallography is one of the characteristics that can influence the shape of a precipitate, but its influence is usually overwhelming when the precipitation occurs in the solid state. In some circumstances, it is symmetry which determines the shape of precipitates which form inside a solid.

Suppose that G_m and G_p represent the symmetry groups of the matrix and precipitate respectively. The common symmetry (intersection group) between these two phases in the observed orientation relationship is defined as H . Given a planar interface between them, symmetry operations consistent with H leads to other orientations of the interface until the particle is fully enclosed and its shape defined. Note that any operation of H is a symmetry operation of the parent and product and hence each crystal orientation is brought into congruence so the orientation of the two crystals is not affected by H .

Aluminium has the space group $Fm\bar{3}m$ and the silver-rich precipitate Ω has the space group $Fmmm$. The orientation relation has been measured to be:

$$[001]_{\Omega} \parallel [111]_{\text{Al}}$$

$$[100]_{\Omega} \parallel [10\bar{1}]_{\text{Al}}$$

Fig. 4.5 shows the stereograms of the symmetry elements of the two crystals, in the correct relative orientation and it is evident the common point group symmetry is $2/m$, which is consistent with the observed plate shape of the Ω both with respect to the diad and the mirror plane.

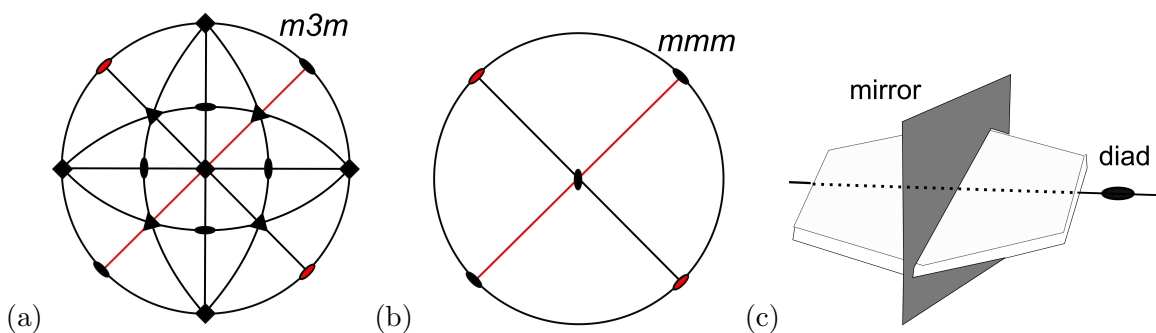


Figure 4.5: (a) Stereographic representation of the symmetry elements in the point group $m\bar{3}m$ for aluminium. (b) Stereographic representation of the symmetry elements in the point group mmm for Ω . The symmetry elements shared by Al and Ω are highlighted in red. (c) The precipitate shape observed, corresponding to the shared symmetry group $2/m$.

4.6 Summary

We have touched on the notion of space groups which represent all the symmetry elements of the crystal. The appreciation of space groups is essential in the solution of structures, transformations which lead to changes in symmetry, and the properties of crystals. A great deal of the work in identifying the number of symmetry related positions as a function of the space group has already been documented, with the information routinely available either from the tables published by the International Union of Crystallography or via the world wide web.

Chapter 5

The Reciprocal Lattice and Diffraction

5.1 The Reciprocal Basis

The basis vectors \mathbf{a}_i were defined in Chapter 1; a vector \mathbf{u} in real space can then be written as a linear combination of the basis vectors:

$$\mathbf{u} = u_1\mathbf{a}_1 + u_2\mathbf{a}_2 + u_3\mathbf{a}_3,$$

where u_1 , u_2 and u_3 are its components, when \mathbf{u} is referred to the basis A.

The reciprocal lattice constitutes a special co-ordinate system, designed originally to simplify the study of diffraction phenomena. If we consider a lattice, represented by a basis symbol ‘A’ and an arbitrary set of non-coplanar basis vectors \mathbf{a}_1 , \mathbf{a}_2 and \mathbf{a}_3 , then the corresponding reciprocal basis A^* has basis vectors \mathbf{a}_1^* , \mathbf{a}_2^* and \mathbf{a}_3^* , defined by the following equations:

$$\mathbf{a}_1^* = (\mathbf{a}_2 \wedge \mathbf{a}_3) / (\mathbf{a}_1 \cdot \mathbf{a}_2 \wedge \mathbf{a}_3)$$

$$\mathbf{a}_2^* = (\mathbf{a}_3 \wedge \mathbf{a}_1) / (\mathbf{a}_1 \cdot \mathbf{a}_2 \wedge \mathbf{a}_3)$$

$$\mathbf{a}_3^* = (\mathbf{a}_1 \wedge \mathbf{a}_2) / (\mathbf{a}_1 \cdot \mathbf{a}_2 \wedge \mathbf{a}_3)$$

The term $(\mathbf{a}_1 \cdot \mathbf{a}_2 \wedge \mathbf{a}_3)$ represents the volume of the unit cell formed by \mathbf{a}_i , while the magnitude of the vector $(\mathbf{a}_2 \wedge \mathbf{a}_3)$ represents the area of the $(1\ 0\ 0)_A$ plane (Fig. 5.1). Since $(\mathbf{a}_2 \wedge \mathbf{a}_3)$ points along the normal to the $(1\ 0\ 0)_A$ plane, it follows that \mathbf{a}_1^* also points along the normal to $(1\ 0\ 0)_A$ and that its magnitude $|\mathbf{a}_1^*|$ is the reciprocal of the spacing of the $(1\ 0\ 0)_A$ planes (Fig. 5.1).

The components of any vector referred to the reciprocal basis represent the Miller indices of a plane whose normal is along that vector, with the spacing of the plane given by the inverse of the

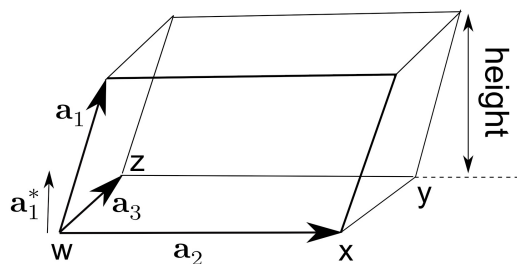


Figure 5.1: The relationship between \mathbf{a}_1^* and \mathbf{a}_i . The vector \mathbf{a}_1^* lies normal to the basal plane $wxyz$ and the volume of the parallelepiped formed by the basis vectors \mathbf{a}_i is given by $\mathbf{a}_1 \cdot \mathbf{a}_2 \wedge \mathbf{a}_3$. The area of the basal plane is $|\mathbf{a}_2 \wedge \mathbf{a}_3|$. The height is the spacing between planes parallel to the basal plane, given by $1/|\mathbf{a}_1^*|$.

magnitude of that vector. For example, the vector $(\mathbf{u}; A^*) = (1\ 2\ 3)$ is normal to planes with Miller indices $(1\ 2\ 3)$ and interplanar spacing $1/|\mathbf{u}|$. We see that

$$\mathbf{a}_i \cdot \mathbf{a}_j^* = 1 \quad \text{when } i = j, \quad \text{and} \quad \mathbf{a}_i \cdot \mathbf{a}_j^* = 0 \quad \text{when } i \neq j \quad (5.1)$$

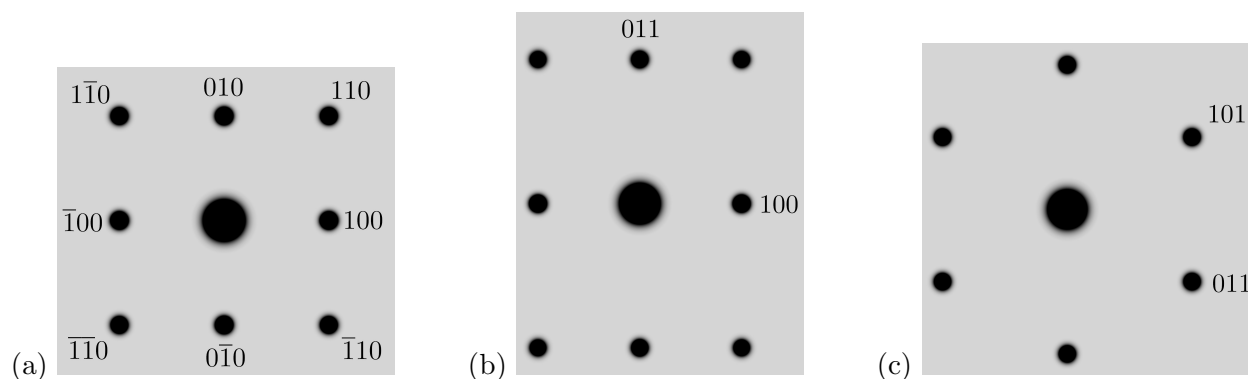


Figure 5.2: Sections of the reciprocal lattice of a cubic-P lattice. (a) Section normal to $[001]$. (b) Section normal to $[01\bar{1}]$. (c) Section normal to $[\bar{1}\bar{1}\bar{1}]$. Notice how the distance varies inversely with the spacing of the planes. The origin of the reciprocal lattice is not labelled, but if necessary, can be designated 000.

5.2 Crystallography of diffraction

Consider waves of length λ incident on planes of atoms. The beams reflected from *different* planes in the parallel set illustrated in Fig. 5.3 must also be in phase to avoid destructive interference. Therefore, the path difference between beams a and b , i.e. the distance xyz , must be an integral number of wavelengths. Since $xyz = 2d \sin \theta$, the diffraction condition is

$$n\lambda = 2d \sin \theta \quad (5.2)$$

where n is an integer and this equation is the Bragg law, with θ the Bragg angle.

The Bragg law can be expressed conveniently in terms of vectors in reciprocal space. In Fig. 5.4, the Bragg law is satisfied if

$$\mathbf{k}' - \mathbf{k} = \mathbf{g} \quad (5.3)$$

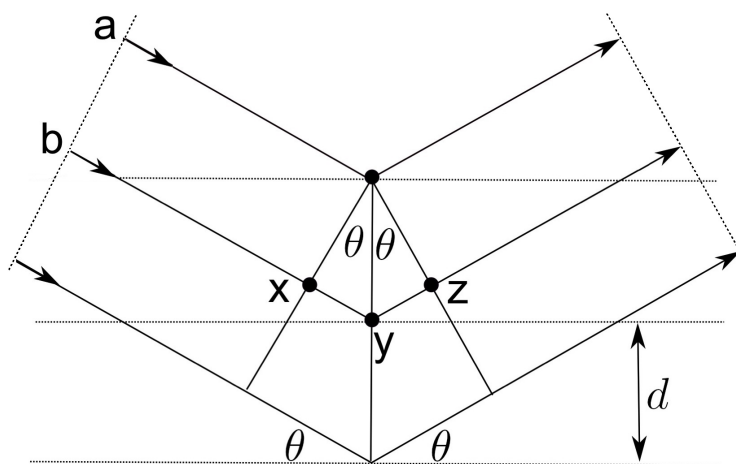


Figure 5.3: Electromagnetic waves incident on a set of parallel crystal planes with an interplanar spacing d . The angle of emergence of the scattered waves is the same as that of incidence.

Here \mathbf{g} is a reciprocal lattice vector beginning at the origin $(0,0,0)$ and representing the crystal which is being illuminated by the radiation \mathbf{k} . From the geometry of the triangle, it is evident that $\sin \theta = \frac{1}{2}g/k$ so that $\sin \theta = (0.5/d)/(1/\lambda)$ which on rearrangement gives the Bragg law.

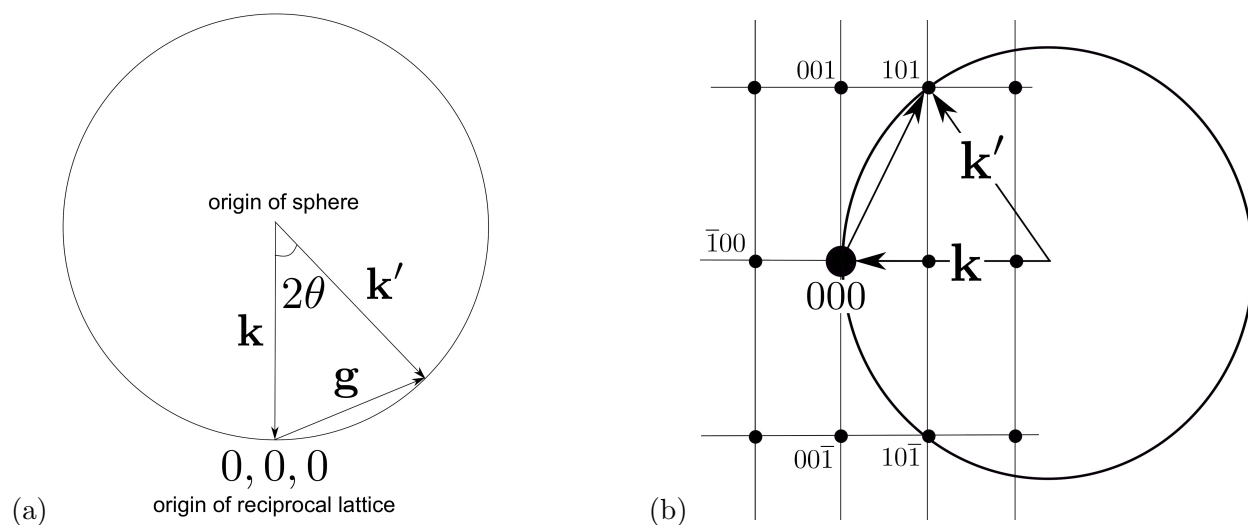


Figure 5.4: (a) The Ewald sphere construction in reciprocal space. \mathbf{k} represents the direction of the incident beam, \mathbf{k}' that of the diffracted beam and \mathbf{g} the normal to the diffracting planes. Both \mathbf{k} and \mathbf{k}' have a magnitude λ^{-1} and \mathbf{g} has a magnitude d^{-1} . The beam is incident on a crystal which is represented by its reciprocal lattice with origin at $0,0,0$. (b) Another illustration of the Ewald sphere superimposed on the reciprocal lattice. In this case only the 101 and $10\bar{1}$ planes are in Bragg condition. The reciprocal lattice vectors which do not touch the sphere are not in Bragg orientation.

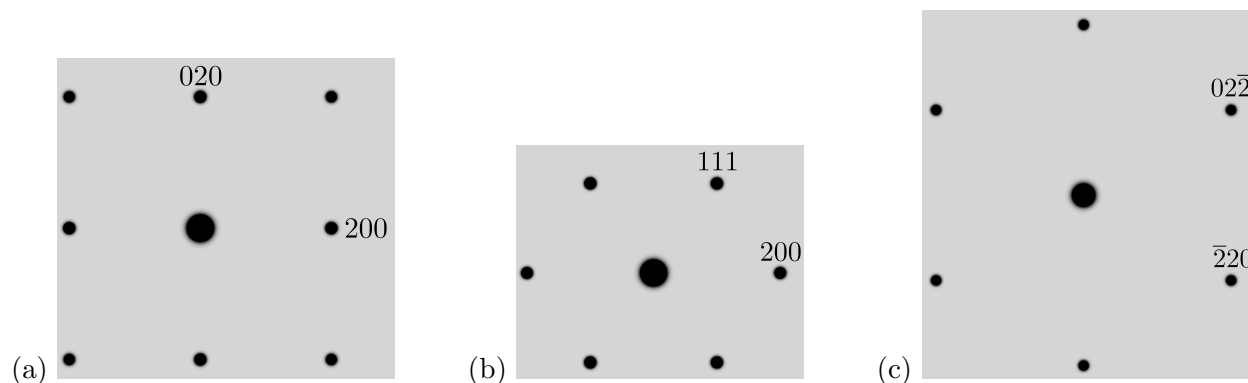


Figure 5.5: Electron diffraction patterns from austenite (cubic-F). (a) Zone axis parallel to $[001]$. (b) Zone axis parallel to $[0\bar{1}1]$. (c) Zone axis parallel to $[111]$. Notice that in any pattern, one only needs to index two reciprocal lattice vectors in order for all the others to be determined. In the cases illustrated, the symmetry of the patterns is consistent with that of the zone axes. Contrast these patterns with the reciprocal lattice sections presented in Fig. 5.2.

5.3 Intensities

The electrons from an individual atom can coherently scatter an X-ray beam; the atomic scattering factor f is the ratio of the amplitude scattered by an atom to that scattered by one electron. We are interested in coherent scattering by all the atoms in a unit cell, in which case the resultant for reflections from hkl planes is given by a summation known as the *structure factor*:

$$\begin{aligned}
 F_{hkl} &= \sum_1^{n \text{ atoms}} f_n \exp\{2\pi i(hu_n + kv_n + lw_n)\} \\
 &\equiv \sum_1^{n \text{ atoms}} f_n [\cos 2\pi(hu_n + kv_n + lw_n) + i \sin 2\pi(hu_n + kv_n + lw_n)]
 \end{aligned} \tag{5.4}$$

where f_n is the scattering factor of atom n and the sum is over all atoms in the unit cell.[†] The magnitude $|F|$ is now the ratio of the amplitude scattered by a unit cell to that scattered by one electron. $|F|^2$ is proportional to the scattered intensity. Notice that for a centrosymmetric system, the sine term can be neglected since that function is not symmetric about zero. As an example, for the structure of Cu (cubic close-packed, with four atoms in the cell at 000 , $\frac{1}{2}\frac{1}{2}0$, $\frac{1}{2}0\frac{1}{2}$, and $0\frac{1}{2}\frac{1}{2}$),

$$F = f[1 + e^{\pi i(h+k)} + e^{\pi i(h+l)} + e^{\pi i(k+l)}] \tag{5.5}$$

so that the $\{100\}$ and $\{110\}$ reflections would have zero structure factor.

Techniques in which the atomic scattering factor scales with the atomic number include electron and X-ray diffraction. Reflections such as $\{100\}_\delta$ that are dependent on the differences in the atomic scattering factors of unlike species, will therefore be weak. In neutron diffraction, the scattering

[†] $e^{\pi i} = e^{3\pi i} = -1$, $e^{2\pi i} = e^{4\pi i} = +1$, $e^{\pi i/2} = i$, $e^{3\pi i/2} = -i$, $(1+i)(1-i) = 2$

factors can be quite different for atoms with similar atomic numbers so superlattice reflections can be more readily detected.

5.4 Diffraction from Thin Crystals

When an incident beam deviates by $\Delta\theta$ from the ideal Bragg angle θ consistent with equation 5.2, it is possible to find another beam from within the depth of the crystal which has a path difference of $\frac{1}{2}\lambda$ and which will destructively interfere with it. This depth, needed to find the wave which is out of phase, increases as $\Delta\theta$ becomes smaller; hence for thin crystals, it may not be possible to destroy deviant rays. For thin crystals it becomes possible to obtain diffracted intensity even when the incident beam is not at the exact Bragg orientation.

In transmission electron microscopy we are constrained to work with thin foils. It follows that diffraction becomes possible even when the incident electron beam is not at the exact Bragg orientation. We express this on the Ewald sphere construction by extending the reciprocal lattice points in the direction normal to the thin foil (Fig. 5.6, 5.7, 5.8). The fact that electrons have a very small wavelength compared with X-rays also helps achieve a greater chance of diffraction because the Ewald sphere is then relatively flat.

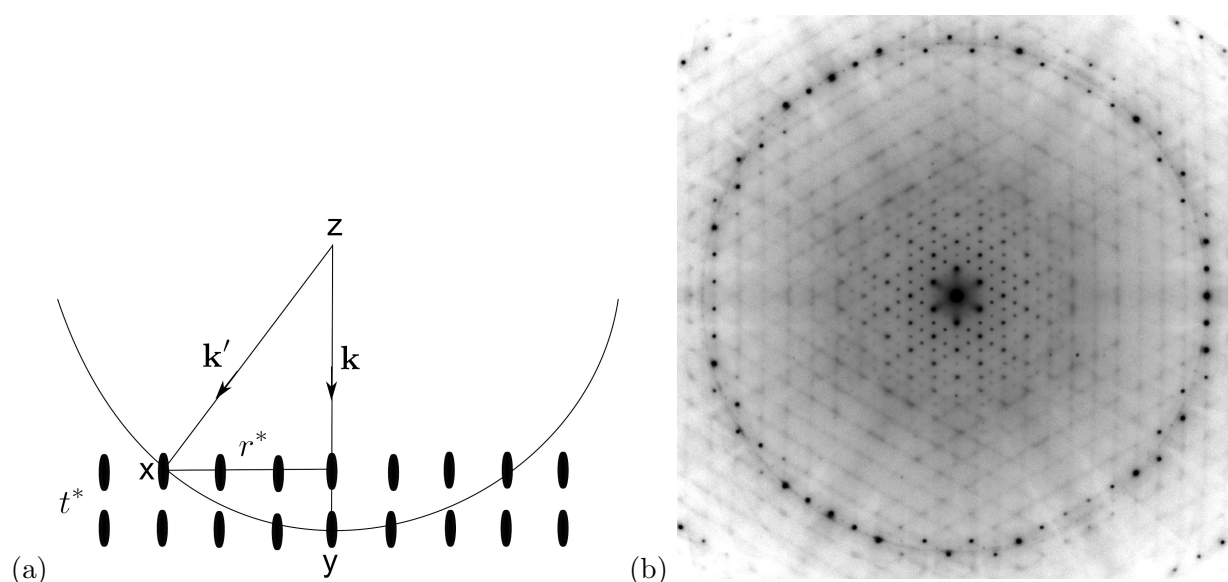


Figure 5.6: (a) Ewald sphere construction for diffraction from a thin foil. The origin of the reciprocal lattice is at 'O' and the layer designated 'P' is the next layer normal to the incident beam, a distance $1/t^*$ from the first layer. (b) $\langle 111 \rangle$ axis ReO_3 showing the higher order Laue zone (the second layer of the type sketched in (a).) - pattern courtesy of P. Midgley.

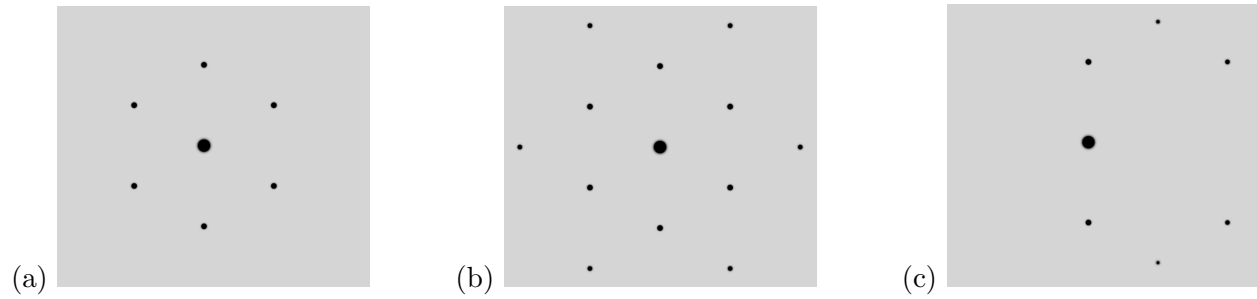


Figure 5.7: Fe with cubic-F structure. (a) Electron diffraction from a foil which is 200 nm thick, zone axis $[111]$. (b) Diffraction from the same foil after thinning it to just 50 nm thickness, zone axis $[111]$. Because of this minute thickness, it becomes possible to pick up reflections from planes of the form $\{224\}$. (c) as (a) but zone axis $[1\ 1\ 0.9]$. The Ewald sphere is now tilted away from some of the reciprocal lattice points on the left hand side.

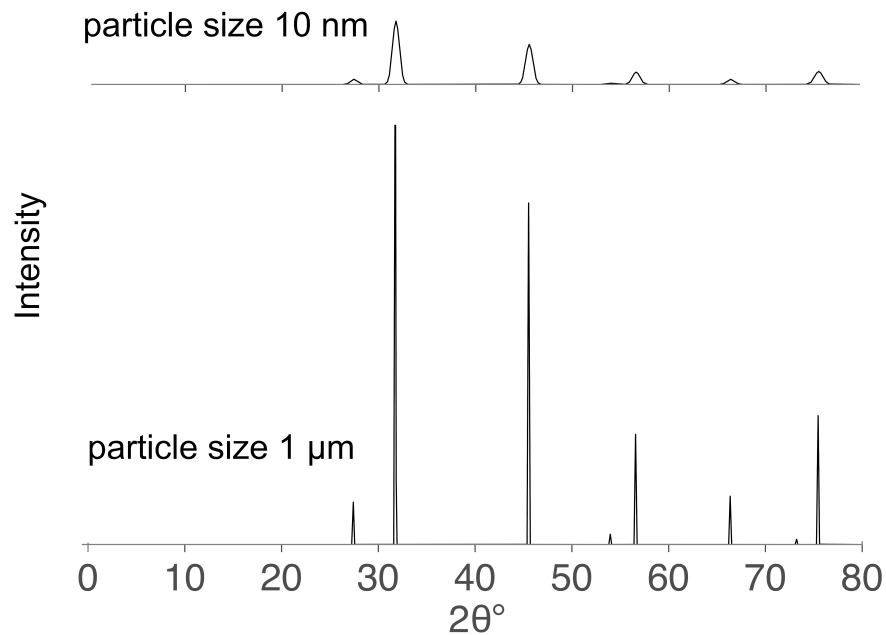


Figure 5.8: The effect of crystal size (in all directions) on an X-ray diffraction pattern. The material concerned is halite. The peaks broaden as the crystal gets smaller.

5.5 Neutron Diffraction

Neutrons are scattered by the atom nucleus and hence the scattering factor is not sensitive to scattering angle; unlike X-rays, the scattering power does not diminish with the Bragg angle θ , so good results are obtained even at high θ . Also unlike X-rays, there is little correlation between the scattering factor and atomic number. Because the interactions are with the nucleus, it becomes

possible to distinguish between isotopes because they now have different neutron scattering factors (for example, hydrogen and deuterium).

X-rays typically penetrate a few micrometers of the surface of a sample, whereas neutrons can penetrate several centimetres. Residual stress is that which is locked in a sample that is otherwise at equilibrium, with no externally applied stress. Fig 5.9 shows residual stress contours that are determined by measuring lattice spacings, comparing them with a stress-free sample to calculate strains, and then converting strains into stresses using the elastic properties of the material.

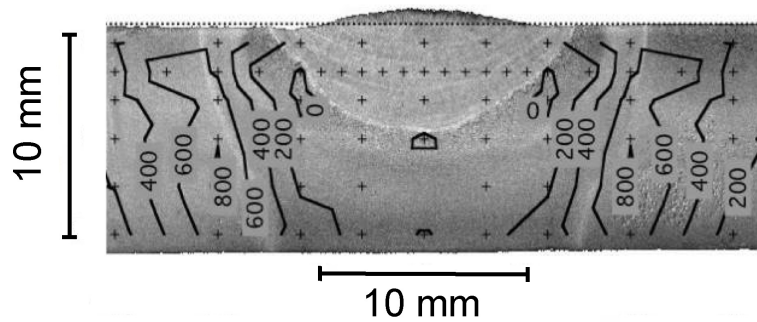


Figure 5.9: Stress distribution in a steel weld determined using neutron diffraction. This would not be possible using X-rays. The numbers on the contours represent MPa.

5.6 Summary

It takes a leap of imagination to understand why it is necessary to deal with a space in which dimensions are inverted. But the fact is that in crystallography, it can be regarded simply as a lattice in which all reciprocal lattice vectors represent normals to planes in real space, with the magnitudes of these vectors representing the inverse of the spacing of those planes. Whereas a plane in real space is defined by a pair of vectors that lie in that plane, in reciprocal space the plane is represented by a vector. A plane in reciprocal space represents all real space planes that share a common direction (a zone axis).

Imagine now that we wish to find a direction that is parallel to a plane normal. This is trivial for a cubic system where plane normals and directions with the same indices are parallel. So a $[123]$ direction is parallel to the normal of the (123) plane. This is not generally true for non-cubic systems, but there exists a metric tensor which makes it easy to find vectors in reciprocal space that are parallel to those in real space (and vice versa), a subject reserved for advanced study.

Chapter 6

Deformation and Texture

6.1 Slip in a Single-Crystal

In a tensile test on the sample of cross-sectional area A illustrated in Fig. 6.1a, the normal to the slip plane lies at an angle ϕ to the force F , and the slip direction is at an angle λ to the tensile axis. The area of the slip plane is $A/\cos\phi$ and the force in the slip direction is $F\cos\lambda$ so that the shear stress on the slip plane in the slip direction is

$$\tau = \frac{F}{A} \underbrace{\cos\phi \cos\lambda}_{\text{Schmid factor}} \quad (6.1)$$

The Schmid factor has a maximum value of 0.5 when $\phi = \lambda = 45^\circ$. Suppose that a tensile axis is along $[213]$, plotted on the shaded stereographic triangle in Fig. 6.1b. There is a simple way of determining which slip system will have the largest resolved shear stress. The slip system will be defined by a slip plane and a slip direction with the latter lying in the former. This means that the two components of the slip system must come from different stereographic triangles. The two stereographic triangles that are adjacent to the shaded triangle satisfy this condition. Any other combination gives angles that are too large, giving Schmid factors that are smaller. The slip system with the highest resolved shear stress when the tensile axis lies in the shaded triangle will therefore be $[011](1\bar{1}1)$. The construction illustrated is known as Diehl's rule.

The unconstrained shear deformation of a single crystal as illustrated in Fig. 6.2 leads to the rotation of the axis along which the force is applied. The normal to the slip plane, the tensile axis and the slip direction are all in the same plane and remain so during rotation. The tensile axis rotates towards the slip direction, on this common plane, during the course of deformation. If the axis along which the force is applied is not allowed to change orientation, then it is the slip system which rotates during deformation Fig. 6.2.

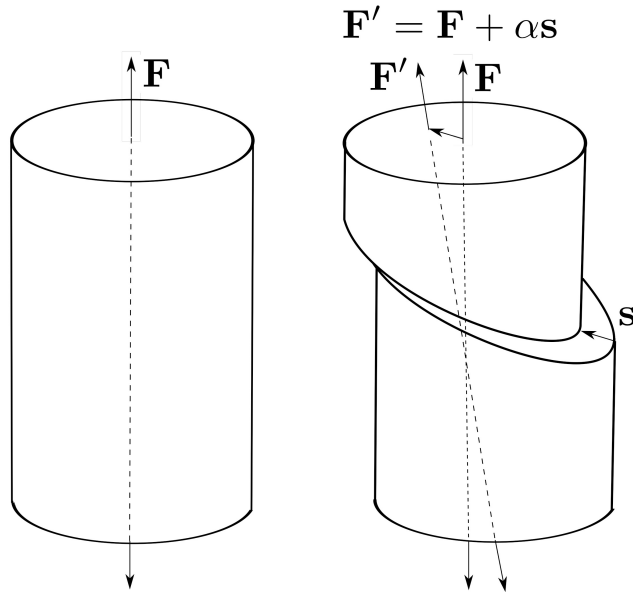


Figure 6.2: Slip of an unconstrained single-crystal. Notice how the axis along which the force is applied rotates as a consequence of the slip. The amount of shear implemented is written αs . If the force axis is constrained to be vertical then the sample will rotate relative to the testing machine by the extent illustrated.

6.2 Texture

Imagine that there is a polycrystalline substance in which the individual crystals are randomly oriented relative to an *external frame of reference*[‡]. Suppose that this polycrystalline substance is subjected to rolling deformation. The individual crystals will then tend to rotate such that the slip planes comply with the external forces as illustrated in Fig. 6.2. This means that the original random distribution of crystals in the undeformed sample becomes non-random. The deformed material is said to become *crystallographically textured*.

Most polycrystalline materials show texture due to processing. Texture can arise during solidification when those crystals which have a fast growth direction parallel to that of the heat flow will dominate the final structure. It can arise during recrystallisation and phase transformation when selective nucleation leads to the formation of a biased distribution of crystals.

A convenient method for communicating texture caused by deformation, for example, in rolled sheet, is by stating the set $\{h k l\}\langle u v w \rangle$, the planes which lie roughly parallel to the rolling plane, and direction in the rolling plane that tends to be parallel to the rolling direction. The overall texture can be represented as the sum of components:

$$\text{texture} = \sum_i \lambda_i \{h k l\}_i \langle u v w \rangle_i \quad (6.2)$$

where λ represents the weighting given to a particular type of texture. The major components of the deformation texture of austenite are $\{1 1 0\}\langle 1 \bar{1} 2 \rangle$ and $\{1 1 2\}\langle 1 1 \bar{1} \rangle$, the so-called *brass*

[‡]This frame may, for example, consist of a set of vectors parallel to the rolling direction, transverse direction and thickness of a rolled plate; alternatively, the principal axes of an applied system of stresses.

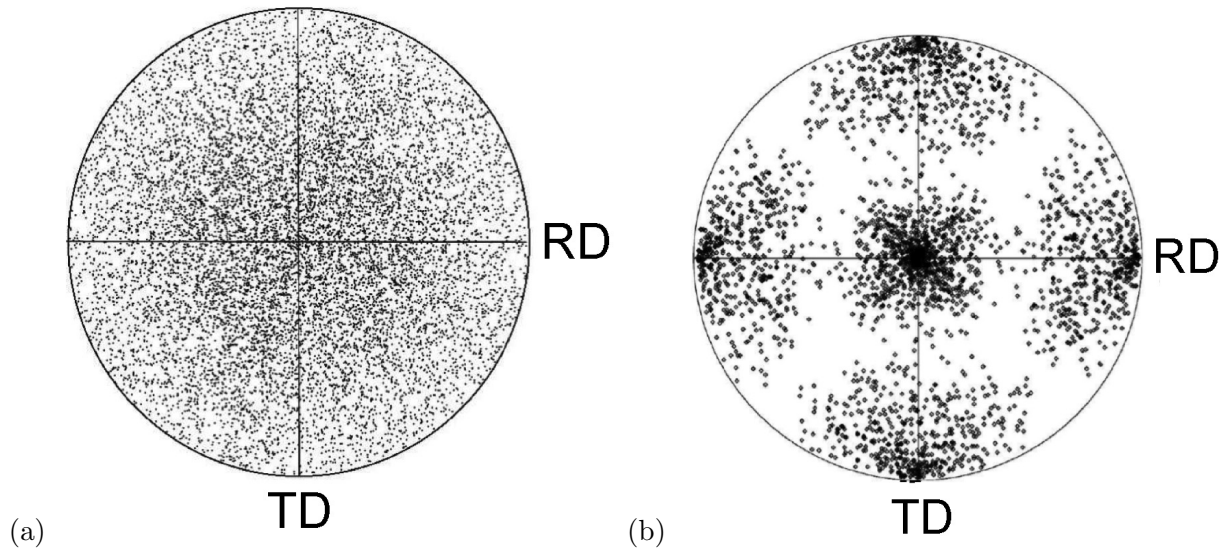


Figure 6.3: (a) Figure showing a random distribution of 100 poles from a polycrystalline sample containing 500 crystals, plotted relative to the rolling direction (RD) and transverse direction (TD). Notice that the distribution of poles does not appear random but this is an artefact due to the angular distortion on a stereographic projection. (b) Corresponding pole figure after texture is introduced by phase transformation. Here there is a strong tendency for the 100 poles to cluster around the sample axes. The distribution of poles can be plotted as contours rather than the dots illustrated.

and *copper* textures respectively. Recrystallisation in a ferritic steel often leads to a *cube* texture $\{1\ 0\ 0\}\{0\ 0\ 1\}$ *cube* component and special thermomechanical processing of the type used to produce magnetically soft metal is associated with the *Goss texture* $\{1\ 1\ 0\}\{0\ 0\ 1\}$.

Texture can be plotted on a stereogram. A *pole figure* in this context consists of a stereogram with its axes defined relative to the external frame of reference, and with particular hkl poles from each of the crystals in the polycrystalline aggregate plotted on to it. If the distribution of crystals is random, the pole figure would appear as in Fig. 6.3a, and if the distribution is non-random then this would be apparent in the pole figure, as shown in Fig. 6.3b.

An *inverse pole figure* is one in which the sample frame is plotted relative to the crystal axes of a reference crystal. Fig. 6.4 an example where the rolling, normal and transverse directions (RD , ND and TD respectively) are plotted relative to the crystal axes as defined by the stereographic triangle. In a cubic system, the 24 stereographic triangles with $\langle 100 \rangle$, $\langle 101 \rangle$, and $\langle 111 \rangle$ at the corner of each triangle, are crystallographically equivalent. Therefore, the orientation of the rolling direction, for example, from each of the 24 triangles can be plotted on just one of the stereographic triangles in the form of poles, or contour plots representing the design of poles in angular space.

Crystallographic texture can be measured using a variety of techniques such as X-ray diffraction or electron back-scattered diffraction (EBSD). In the former case, the polycrystalline sample is

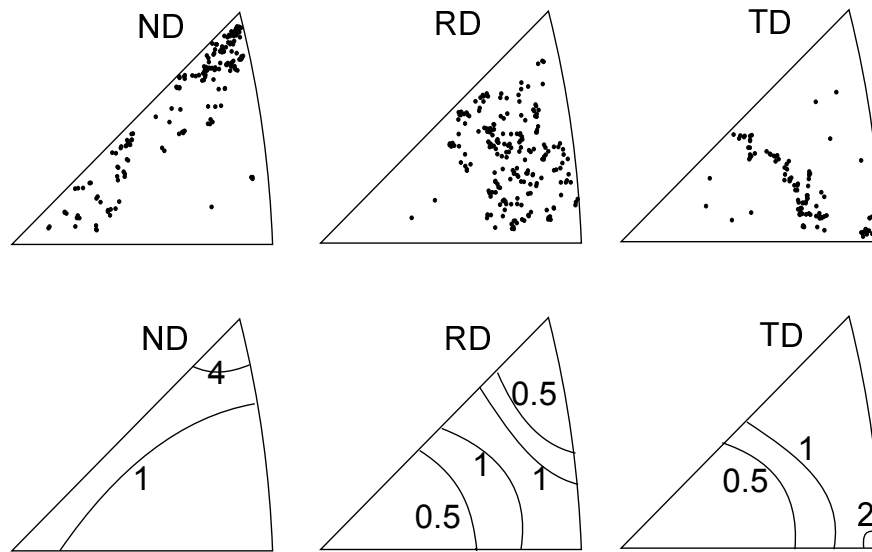


Figure 6.4: Inverse pole figures for a cubic crystal. The diagrams at the top have poles corresponding to the rolling, normal and transverse directions plotted relative to the crystal axes, whereas those at the bottom have the same data represented as contours representing the density of poles.

exposed in a system set to detect X-rays from a particular reflection (Bragg angle) and the sample is systematically tilted and rotated in order to capture intensity at a variety of orientations. In EBSD, an electron beam is rocked about a fixed point on the surface of a grain using a scanning electron microscope. At particular angles, the beam is Bragg diffracted, resulting in a reduction in intensity picked up by the detector, leading to the formation of channelling patterns of the type illustrated in Fig. 6.5. These patterns can be interpreted to determine the orientation of the crystal relative to the sample axes.

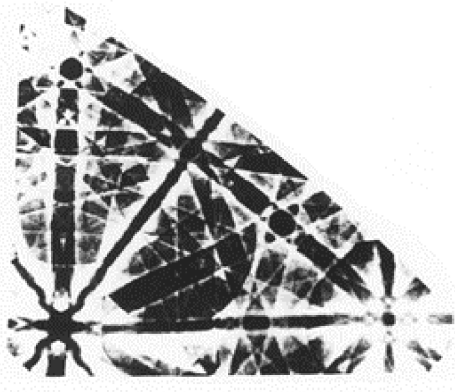


Figure 6.5: An electron channelling pattern from a crystal of copper plotted on a standard stereographic triangle.

6.3 Orientation Distribution Functions

A pole figure does not give information about the orientation of a particular crystal relative to another, since the poles are not in the final plot identified with particular crystals. An orientation distribution function is a more rigorous method of expressing the orientations of crystals relative to the frame of reference. It uses three Euler angles (φ_1 , Φ and φ_2) which define the relative orientation of the crystal and sample frames of reference, as illustrated in Fig. 6.6.

The set of measured Euler angles made by the *RD*, *TD* and *ND* directions for a particular crystal is plotted as a point in a cube whose axes scale with φ_1 , Φ and φ_2 . Each point inside this cube is a single crystal.

There are very many industrial processes which control and exploit texture on a grand scale. Beverage cans are incredibly thin even though their bodies are made without fracture using extreme deformation including deep drawing. The texture of the material prior to drawing is controlled such that plastic instability is avoided in the thickness direction. For similar reasons, the steels used in the manufacture of formed automobile bodies are texture-controlled. Iron alloys used to make electricity transformers have to be magnetically soft. This is achieved by controlling the crystallographic texture to minimise magnetic losses.

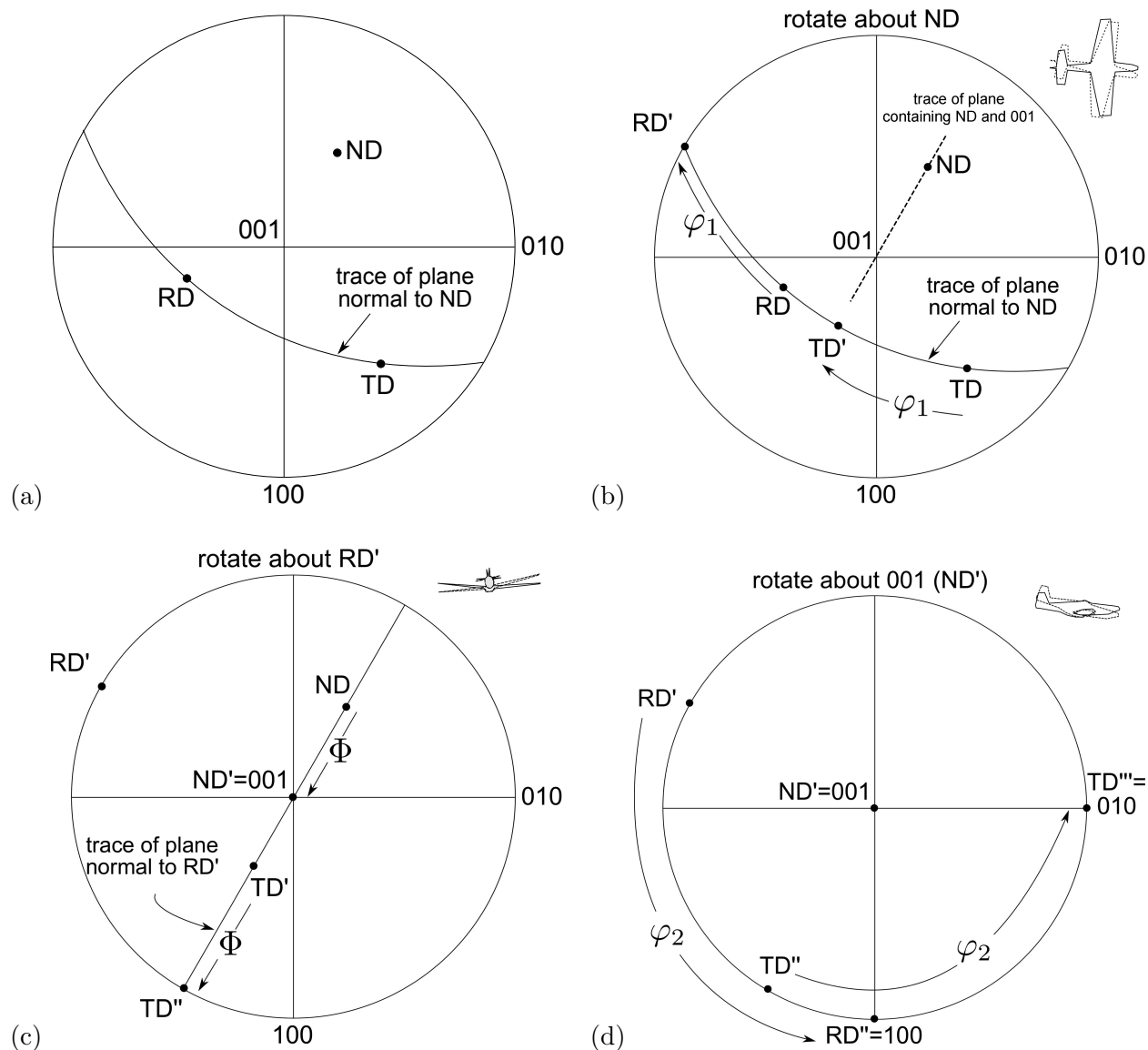


Figure 6.6: Operations that define the three (Bunge) Euler angles. (a) Initial relationship between crystal and sample coordinates. (b) Rotation by φ_1 about ND to generate RD' in a position normal to the plane containing ND and 001. (c) Rotate by Φ about RD' to generate ND' parallel to 001. (d) Rotate by φ_2 about 001 to bring crystal and sample axes into coincidence. The insets show the rotations relative to an aircraft.

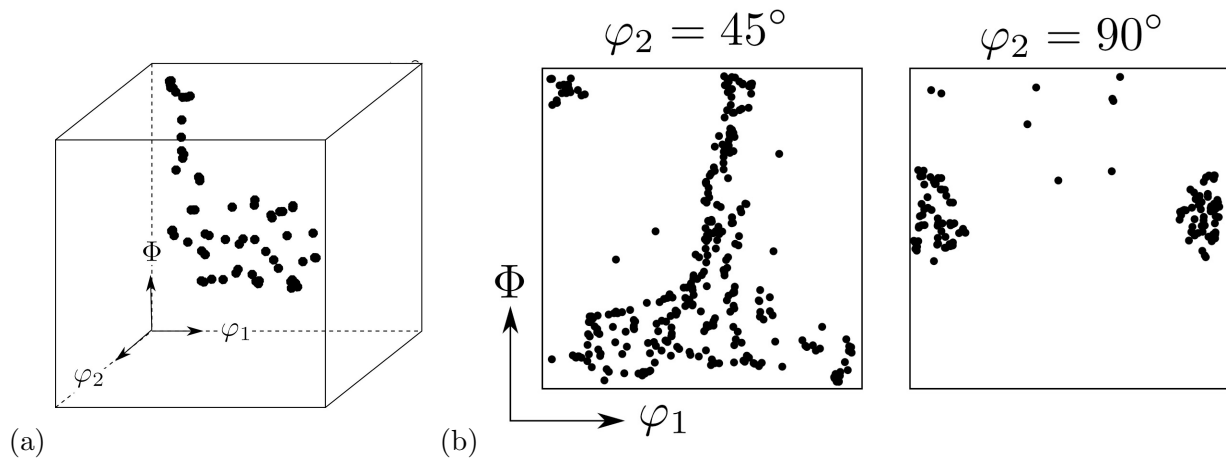


Figure 6.7: (a) An orientation distribution plotted on a cube with axes defined by the Euler angles. Each dot represents a crystal orientation relative to sample axes. (b) Sections of the cube to show how the density of orientations varies.

6.4 Summary

Crystallographic texture can be understood by a thought experiment in which a large single crystal is broken up into many smaller ones which are then joined together in somewhat different orientations that are not random. The material then behaves as if it has some of the characteristics of a single crystal (such as anisotropy) while other properties are more a feature of random polycrystals (such as the multiple slip systems needed per crystal in order to achieve plasticity without the creation of voids).

We have discussed how texture can arise from plastic deformation, but any kind of processing can lead to its development. The heat treatment of deformed materials to induce recrystallisation can lead to recrystallisation textures because not all ‘nuclei’ grow at the same rate. The nuclei have to be sufficiently different in orientation from their surroundings to accomplish rapid growth. Similar selection can occur in phase transformations where the product phase forms at a grain boundary because certain boundaries make it possible for the product to adopt a favourable orientation relationship with the parent phase on either side of the interface. Both magnetic and electrical fields can also lead to orientational order in appropriate materials.

So how does one produce a polycrystalline material with a random arrangement of grains? The short answer is, with enormous difficulty. Powder techniques can partially reach this goal; metallic or ceramic powders that are sintered together tend to undergo very limited deformation or rotation during fabrication, and hence may approach a random orientational distribution.

Chapter 7

Interfaces, Orientation Relationships

7.1 Introduction

Much of the science and technology of polycrystalline materials depends on the nature of interfaces between crystals and the relative orientations of adjacent crystals. The corrosion resistance of a boundary depends on how coherent it is, the continuity of deformation depends on the relative orientations of the adjacent crystals ... the list is seemingly endless!

Atoms in the boundary between crystals must in general be displaced from positions they would occupy in the undisturbed crystal, but it is now well established that many interfaces have a periodic structure. In such cases, the misfit between the crystals connected by the boundary is not distributed uniformly over every element of the interface; it is periodically localised into discontinuities which separate patches of the boundary where the fit between the two crystals is good or perfect. When these discontinuities are well separated, they may individually be recognised as interface dislocations which separate coherent patches in the boundary, which is macroscopically said to be semi-coherent. The simple example of a symmetrical tilt boundary illustrates this.

7.2 Symmetrical Tilt Boundary

The structure of an interface can be understood by creating a boundary beginning with a single crystal that is sliced and the two halves then rotated relative to generate two crystal in different orientations. The rotation illustrated in Fig. 7.1 about an axis normal to the diagram through an angle θ . This leaves a gap between the bicrystal which can be filled with edge dislocations that after all, have extra half-planes. The misorientation θ between the grains can therefore be described in terms of dislocations. Inserting an edge dislocation of Burgers vector \mathbf{b} is like forcing a wedge into the lattice, so that each dislocation is associated with a small change in the orientation of the

lattice on either side of the extra half plane. If the spacing of dislocations is d , then it follows from Fig. 7.1b that

$$\tan \frac{\theta}{2} = \frac{b}{2d} \quad (7.1)$$

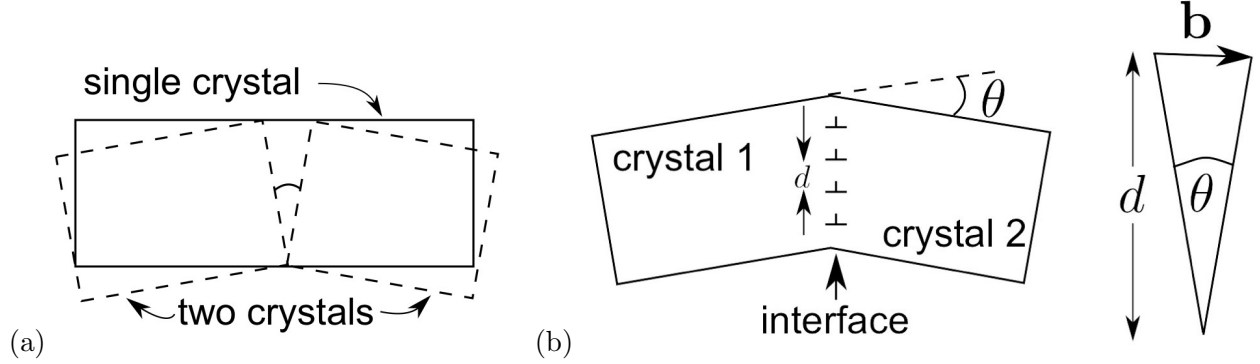


Figure 7.1: The creation of an interface. (a) Single crystal cut in two halves which are then tilted through an angle θ about an axis normal to the diagram. (b) The gap within the tilt is filled with edge dislocations, each with a Burgers vector \mathbf{b} and spacing d to create an interface.

The structure of the interface in terms of dislocations provides a mechanism for calculating the energy per unit area of the interface as a function of the misorientation θ . The energy per unit length W_s of a dislocation is given by:

$$\begin{aligned} W_s &= W_c + \frac{1}{2} \int_{r_0}^{r_\infty} \frac{Gb^2}{2\pi(1-\nu)} \frac{dr}{r} \\ &= W_c + \frac{Gb^2}{4\pi(1-\nu)} \ln \left\{ \frac{r_\infty}{r_0} \right\} \end{aligned} \quad (7.2)$$

where W_c is the core energy per unit length, covering the region of the dislocation where elasticity theory fails; G and ν are the shear modulus and Poisson's ratio respectively; r_0 is the radius of the dislocation core and r_∞ is a cut-off radius beyond which the dislocation strain field can be neglected or is limited by the size of the sample. In arrays of dislocations of the type found in interfaces, the strain fields of individual dislocations are partly compensated by their neighbours so it is a good approximation that $r_\infty \approx d$ in which case $r_\infty \propto 1/\theta$. It follows that equation 7.2 can be written $W_s = A(B - \ln \theta)$. Therefore, the interfacial energy per unit area σ_i is related to the number of dislocations per unit area ($1/d$):

$$\begin{aligned} \sigma_i &= \frac{1}{d} \times W_s \\ &= \frac{2}{b} \tan \frac{\theta}{2} \times A(B - \ln \theta) \end{aligned} \quad (7.3)$$

This gives a model for the energy of grain boundaries, based on the density of dislocations in the boundary ($\propto d^{-1}$). The variation in energy as a function of misorientation in the symmetrical tilt boundary described above is illustrated in Fig. 7.2. The model is not valid for large misorientations

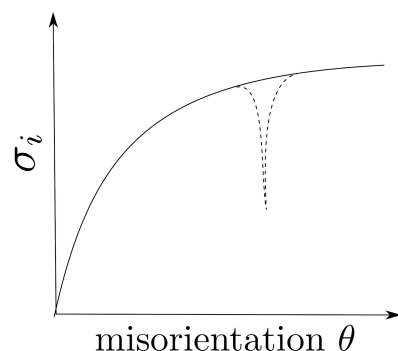


Figure 7.2: The interfacial energy as a function of the misorientation for a tilt boundary. The dashed curve represents cusps when the orientation forms a coincidence site lattice.

where the dislocation spacing becomes comparable with the magnitude of the Burgers vector, since the dislocation cores then begin to overlap.

The symmetrical tilt boundary is an illustration of how interfaces can be described in terms of defect structures with coherent patches in-between the defects. More complex misorientations would require more than one array of dislocations to represent the fit between the crystals, and there will come a point where the defect density becomes so large that it is no longer reasonable to talk of a dislocation structure.

7.3 Coincidence Site Lattices

For high-misorientation boundaries, the predicted spacings of dislocations may turn out to be so small that the misfit is highly localised with respect to the boundary, and the dislocation model of the interface has only formal significance (it is often said that the dislocations get so close to each other that their cores overlap). The arrangement of atoms in such incoherent boundaries may be haphazard, with little correlation of atomic positions across the boundary.

On the other hand, it is unreasonable to assume that all high-angle boundaries have the disordered structure. There is clear experimental evidence which shows that certain high-angle boundaries exhibit the characteristics of low-energy coherent or semi-coherent interfaces; for example, they exhibit strong faceting, have very low mobility in pure materials and the boundary diffusion coefficient may be abnormally low. These observations imply that at certain special relative crystal orientations, which would usually be classified as high-angles orientations, it is possible to obtain boundaries which have a distinct structure - they contain regions of good fit, which occur at regular intervals in the boundary plane, giving a pattern of good fit points in the interface. It is along these points that the two crystals connected by the boundary match exactly.

If we consider the good fit points to correspond to lattice points in the interface which are common to both crystals, then the following procedure allows us to deduce the pattern and frequency of these points for any given orientation relationship. If the two lattices (with a common origin) are

notionally allowed to interpenetrate and fill all space, then there may exist lattice points (other than the origin) which are common to both the crystals. The set of these coincidence points forms a coincidence site lattice (CSL), and the fraction of lattice points which are also coincidence sites is a rational fraction $1/\Sigma$. Σ is thus the reciprocal density of coincidence sites relative to ordinary lattice sites. The value of Σ is a function of the relative orientation of the two grains and not of the orientation of the boundary plane. The boundary simply intersects the CSL and will contain regions of good fit which have a periodicity corresponding to the periodicity of a planar net of the CSL along which the intersection occurs. Boundaries parallel to low-index planes of the CSL are two dimensionally periodic with relatively small repeat cells, and those boundaries with a high planar coincidence site density should have a relatively low energy.

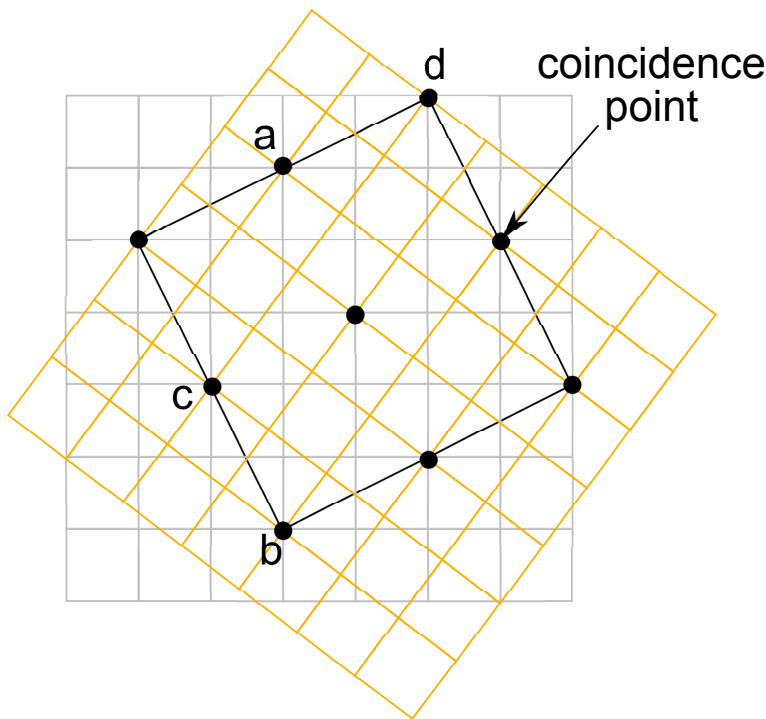


Figure 7.3: A rotation of 36.9° about $\langle 100 \rangle$ of a cubic crystal leads to a $\Sigma 5$. Following any crystal lattice vector leads to coincidence with the other crystal every five vectors, for example, along ‘ab’ or ‘cd’.

7.4 Representation of Orientation Relationships

From Fig. 7.4a, it is evident that the choice of basis vectors \mathbf{a}_i is arbitrary though convenient; Fig. 7.4b illustrates an alternative basis, a body-centred tetragonal (BCT) unit cell describing the same lattice. We label this as basis ‘B’, consisting of basis vectors \mathbf{b}_1 , \mathbf{b}_2 and \mathbf{b}_3 which define the BCT unit cell. It is obvious that $[\mathbf{B}; \mathbf{u}] = [0 \ 2 \ 1]$, compared with $[\mathbf{A}; \mathbf{u}] = [1 \ 1 \ 1]$. The following

vector equations illustrate the relationships between the basis vectors of A and those of B (Fig. 7.4):

$$\begin{aligned} \mathbf{a}_1 &= 1\mathbf{b}_1 + 1\mathbf{b}_2 + 0\mathbf{b}_3 \\ \mathbf{a}_2 &= \bar{1}\mathbf{b}_1 + 1\mathbf{b}_2 + 0\mathbf{b}_3 \\ \mathbf{a}_3 &= 0\mathbf{b}_1 + 0\mathbf{b}_2 + 1\mathbf{b}_3 \end{aligned} \quad (7.4)$$

These equations can also be presented in matrix form as follows:

$$(\mathbf{a}_1 \ \mathbf{a}_2 \ \mathbf{a}_3) = (\mathbf{b}_1 \ \mathbf{b}_2 \ \mathbf{b}_3) \times \begin{pmatrix} 1 & \bar{1} & 0 \\ 1 & 1 & 0 \\ 0 & 0 & 1 \end{pmatrix} \quad (7.5)$$

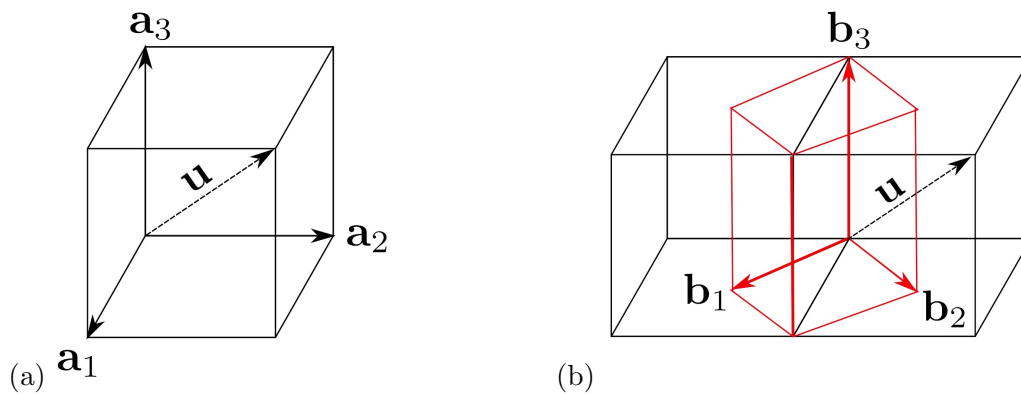


Figure 7.4: (a) Cubic coordinate system with orthogonal basis vectors of equal magnitude. (b) Tetragonal coordinate system (red) in which the basis vectors on the basal plane end at the face-centres of the cubic system (black). The relationship to the cubic cells (black) is also illustrated.

This 3×3 matrix representing the co-ordinate transformation is denoted (B J A) and transforms the components of vectors referred to the A basis to those referred to the B basis. The first column of (B J A) represents the components of the basis vector \mathbf{a}_1 , with respect to the basis B, and so on.

The components of a vector \mathbf{u} can now be transformed between bases using the matrix (B J A) as follows:

$$[\mathbf{B}; \mathbf{u}] = (\mathbf{B} \ \mathbf{J} \ \mathbf{A})[\mathbf{A}; \mathbf{u}] \quad (7.6)$$

Notice the juxtapositioning of like basis symbols. Writing (A J B) as the inverse of (B J A):

$$[\mathbf{A}; \mathbf{u}] = (\mathbf{A} \ \mathbf{J} \ \mathbf{B})[\mathbf{B}; \mathbf{u}]$$

7.5 Co-ordinate transformation

Suppose that two adjacent crystals that have an identical cubic lattice, are represented by bases ‘A’ and ‘B’ respectively. The basis vectors \mathbf{a}_i of A and \mathbf{b}_i of B respectively define the cubic unit cells of the crystals concerned. The lattice parameter is a so that $|\mathbf{a}_i| = |\mathbf{b}_i| = a$. The grains are orientated such that $[0\ 0\ 1]_A \parallel [0\ 0\ 1]_B$, and $[1\ 0\ 0]_B$ makes an angle of 45° with both $[1\ 0\ 0]_A$ and $[0\ 1\ 0]_A$, with $[001]_A \parallel [001]_B$, as illustrated in the diagram below. We shall prove that if \mathbf{u} is a vector such that its components in crystal A are given by $[A; \mathbf{u}] = [\sqrt{2}\ 2\sqrt{2}\ 0]$, then in the basis B, $[B; \mathbf{u}] = [3\ 1\ 0]$. Show that the magnitude of \mathbf{u} (*i.e.* $|\mathbf{u}|$) does not depend on the choice of the basis.

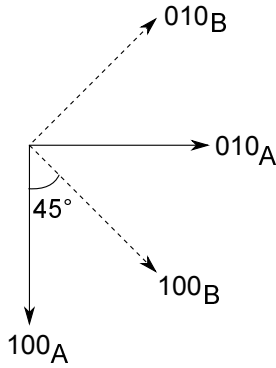


Figure 7.5: Diagram illustrating the relation between the bases A and B. Note that $[001]_A \parallel [001]_B$.

Referring to Fig. 7.5, and recalling that the matrix $(B\ J\ A)$ consists of three columns, each column being the components of one of the basis vectors of A, with respect to B, we have

$$\begin{aligned} [B; \mathbf{a}_1] &= [\cos 45 \quad -\sin 45 \quad 0] \\ [B; \mathbf{a}_2] &= [\sin 45 \quad \cos 45 \quad 0] \\ [B; \mathbf{a}_3] &= [0 \quad 0 \quad 1] \end{aligned} \quad \text{so that} \quad (B\ J\ A) = \begin{pmatrix} \cos 45 & \sin 45 & 0 \\ -\sin 45 & \cos 45 & 0 \\ 0 & 0 & 1 \end{pmatrix}$$

Now, $[B; \mathbf{u}] = (B\ J\ A)[A; \mathbf{u}]$, and on substituting for $[A; \mathbf{u}] = [\sqrt{2}\ 2\sqrt{2}\ 0]$, we get $[B; \mathbf{u}] = [3\ 1\ 0]$. Both the bases A and B are orthogonal so that the magnitude of \mathbf{u} can be obtained using the Pythagoras theorem. Hence, choosing components referred to the basis B, we get:

$$|\mathbf{u}|^2 = (3|\mathbf{b}_1|)^2 + (|\mathbf{b}_2|)^2 = 10a_\gamma^2 \quad (7.7)$$

With respect to basis A,

$$|\mathbf{u}|^2 = (\sqrt{2}|\mathbf{a}_1|)^2 + (2\sqrt{2}|\mathbf{a}_2|)^2 = 10a_\gamma^2 \quad (7.8)$$

Hence, $|\mathbf{u}|$ is invariant to the co-ordinate transformation. This is a general result, since a vector is a physical entity, whose magnitude and direction clearly cannot depend on the choice of a reference frame, a choice which is after all, arbitrary.

7.5.1 General Rotation Matrix

If we represent an axis of rotation as a unit vector, then only three independent quantities are needed to define a misorientation between grains: two components of the axis of rotation, and an angle of rotation. It follows that a rotation matrix must also have only three independent terms. The components of any rotation matrix can be written in terms of a vector $\mathbf{u} = [u_1 \ u_2 \ u_3]$ which lies along the axis of rotation (such that $u_1u_1 + u_2u_2 + u_3u_3 = 1$), and in terms of the right-handed angle of rotation θ as follows:

$$(\text{Y J X}) = \begin{pmatrix} u_1u_1(1-m) + m & u_1u_2(1-m) + u_3n & u_1u_3(1-m) - u_2n \\ u_1u_2(1-m) - u_3n & u_2u_2(1-m) + m & u_2u_3(1-m) + u_1n \\ u_1u_3(1-m) + u_2n & u_2u_3(1-m) - u_1n & u_3u_3(1-m) + m \end{pmatrix} \quad (7.9)$$

where $m = \cos \theta$ and $n = \sin \theta$. The right-handed angle of rotation can be obtained from the fact that

$$J_{11} + J_{22} + J_{33} = 1 + 2 \cos \theta \quad (7.10)$$

and the components of the vector \mathbf{u} along the axis of rotation are given by

$$\begin{aligned} u_1 &= (J_{23} - J_{32})/2 \sin \theta \\ u_2 &= (J_{31} - J_{13})/2 \sin \theta \\ u_3 &= (J_{12} - J_{21})/2 \sin \theta \end{aligned} \quad (7.11)$$

If the rotation axis in equation 7.9 is set to be $[001]_X$ then

$$(\text{Y J X}) = \begin{pmatrix} \cos \theta & \sin \theta & 0 \\ -\sin \theta & \cos \theta & 0 \\ 0 & 0 & 1 \end{pmatrix} \quad (7.12)$$

Since for a symmetry operation the vector before and after the rotation is related by a linear transformation, the trace of the rotation matrix should be an integer; it follows that since $-1 \leq \cos \theta \leq 1$:

$$J_{11} + J_{22} + J_{33} = 1 + 2 \cos \theta = -1, 0, 1, 2, 3 \quad (7.13)$$

or

$$\theta = 2\pi, \frac{2\pi}{2}, \frac{2\pi}{3}, \frac{2\pi}{4}, \frac{2\pi}{6} \quad (7.14)$$

showing that a five-fold rotation axis is not permitted.

7.6 Example of CSL

We now consider a mathematical method of determining the CSL formed by allowing the lattices of crystals A and B to notionally interpenetrate; A and B are assumed to be related by a transformation $(A \ S \ A)$ which deforms the A lattice into that of B; A and B need not have the same crystal structure or lattice parameters, so that $(A \ S \ A)$ need not be a rigid body rotation. Consider a vector \mathbf{u} which is a lattice vector whose integral components do not have a common factor. As a result of the transformation $(A \ S \ A)$, \mathbf{u} becomes a new vector \mathbf{x} such that

$$[A; \mathbf{x}] = (A \ S \ A)[A; \mathbf{u}] \quad (7.15)$$

Of course, \mathbf{x} does not necessarily have integral components in the A basis (*i.e.*, it need not be a lattice vector of A). CSL vectors, on the other hand, identify lattice points which are common to both A and B, and therefore are lattice vectors of both crystals. It follows that CSL vectors have integral indices when referred to either crystal. Hence, \mathbf{x} is only a CSL vector if it has integral components in the basis A. We note that \mathbf{x} always has integral components in B, because a lattice vector of A (such as \mathbf{u}) always deforms into a lattice vector of B.

The meaning of Σ is that $1/\Sigma$ of the lattice sites of A or B are common to both A and B. It follows that any primitive lattice vector of A or B, when multiplied by Σ , must give a CSL vector. $\Sigma\mathbf{x}$ must therefore always be a CSL vector and if equation 7.15 is multiplied by Σ , then we obtain an equation in which the vector \mathbf{u} always transforms into a CSL vector:

$$\Sigma[A; \mathbf{x}] = \Sigma(A \ S \ A)[A; \mathbf{u}] \quad (7.16)$$

i.e. given that \mathbf{u} is a lattice vector of A, whose components have no common factor, $\Sigma\mathbf{x}$ is a CSL vector with integral components in either basis. This can only be true if the matrix $\Sigma(A \ S \ A)$ has elements which are all integral since it is only then that $\Sigma[A; \mathbf{x}]$ has elements which are all integral.

It follows that if an integer H can be found such that all the elements of the matrix $H(A \ S \ A)$ are integers (without a common factor), then H is the Σ value relating A and B.

The rotation matrix corresponding to the rotation 180° about $[1 \ 1 \ 2]_A$ is given by (equation 7.9)

$$(A \ J \ A) = \frac{1}{3} \begin{pmatrix} \bar{2} & 1 & \bar{2} \\ 1 & \bar{2} & 2 \\ 2 & 2 & 1 \end{pmatrix} \quad (7.17)$$

and since 3 is the integer which when multiplied with $(A \ J \ A)$ gives a matrix of integral elements (without a common factor), the Σ value for this orientation is given by $\Sigma = 3$.

Coincidence site lattices have in recent years become popular because of the advent of orientation imaging in the scanning electron microscope. The microscope is usually associated with software

which calculates the Σ value at every junction between two grains. The accuracy of the technique is limited so such Σ maps should be taken with a pinch of salt, and large Σ values are not very meaningful as representations of low-energy boundaries.

Chapter 8

Crystallography of Martensitic Transformations

8.1 Introduction

Martensitic transformations, and displacive transformations in general, remain the only way of making bulk nanostructured materials for engineering applications. The transformation is diffusionless and hence can occur at incredibly low temperatures (*e.g.* $< 4\text{ K}$), or grow at the speed of sound in the material (a few thousand m s^{-1}). There is no composition change when it grows to consume the parent phase.

There are, however, a number of peculiarities associated with martensitic transformations, which are important in the design of alloys. The interface plane between austenite and martensite is known as the *habit plane* and measurements show that the crystallographic indices of that plane are irrational and strange (Table 8.1). Similarly, the orientation relationship between the parent (γ) and product (α'). The formation of martensite involves the coordinated movement of atoms. Whereas the most densely packed planes tend to be parallel, and close-packed directions within those planes tend to be parallel, there are subtle discrepancies which make the orientations irrational. A typical approximate orientation relationship, in this case with α' being body-centred cubic and γ face-centred cubic, is given *approximately* by

$$\begin{aligned} \{1\ 1\ 1\}_{\gamma} \quad || \quad \{0\ 1\ 1\}_{\alpha'} \\ \langle 1\ 0\ \bar{1} \rangle_{\gamma} \quad || \quad \langle 1\ 1\ \bar{1} \rangle_{\alpha'} \end{aligned} \quad (8.1)$$

Another difficulty is that the α'/γ interface has to be glissile, that is, it must be able to move without diffusion. This requires that the interface must contain no more than one set of dislocations. Any more than one array of line vectors can lead to interference between the dislocations which renders the interface sessile. In crystallographic terms, this means that there must be at least one line fully

Table 8.1: Habit plane indices for martensite. The quoted indices are approximate because the habit planes are in general irrational.

Composition /wt.%	Approximate habit plane indices
Low-alloy steels, Fe-28Ni	$\{1\ 1\ 1\}_\gamma$
Plate martensite in Fe-1.8C	$\{2\ 9\ 5\}_\gamma$
Fe-30Ni-0.3C	$\{3\ 15\ 10\}_\gamma$
Fe-8Cr-1C	$\{2\ 5\ 2\}_\gamma$

coherent in the α'/γ interface. The transformation strain relating the two lattices must therefore at a minimum be an *invariant line strain*.

8.2 The Shape Deformation

During martensitic transformation, the pattern in which the atoms in the parent crystal are arranged is *deformed* into that appropriate for martensite, there must be a corresponding change in the macroscopic shape of the crystal undergoing transformation. The dislocations responsible for the deformation are in the α'/γ interface, with Burgers vectors such that in addition to deformation they also cause the change in crystal structure. The deformation is such that an initially flat surface becomes uniformly tilted about the line formed by the intersection of the interface plane with the free surface (Fig. 8.1). Any scratch traversing the transformed region is similarly deflected though the scratch remains connected at the α'/γ interface.

8.3 Bain Strain

We now consider the nature of the strain necessary to transform the f.c.c. lattice of γ into the b.c.c. lattice of α' . Such a strain was proposed by Bain in 1924 and hence is known as the ‘Bain Strain’ (Fig. 8.2). There is a compression along the z axis and a uniform expansion along the x and y axes.

The Bain strain implies the following *rational* orientation relationship between the parent and product lattices:

$$[0\ 0\ 1]_{fcc} \parallel [0\ 0\ 1]_{bcc} \quad [1\ \bar{1}\ 0]_{fcc} \parallel [1\ 0\ 0]_{bcc} \quad [1\ 1\ 0]_{fcc} \parallel [0\ 1\ 0]_{bcc} \quad (8.2)$$

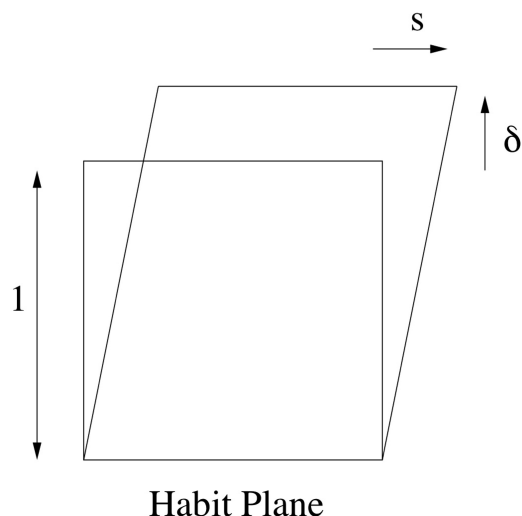


Figure 8.1: The measured shape deformation due to martensitic transformation is an invariant-plane strain with a large shear component ($\simeq 0.22$) and a small dilatational strain ($\simeq 0.03$) directed normal to the habit plane.

but in fact, the experimentally observed orientation relationships are irrational.

The second inconsistency with the Bain strain is that it is not the required invariant-line strain. In Fig. 8.3a,b, the austenite is represented as a sphere which, as a result of the Bain strain \mathbf{B} , is deformed into an ellipsoid of revolution which represents the martensite. There are no lines which are left undistorted or unrotated by \mathbf{B} . There are no lines in the $(0\ 0\ 1)_{fcc}$ plane which are undistorted. The lines wx and yz are undistorted but are rotated to the new positions $w'x'$ and $y'z'$. Such rotated lines are not invariant. However, the combined effect of the Bain strain \mathbf{B} and the rigid body rotation \mathbf{R} is indeed an invariant-line strain (ILS) because it brings yz and $y'z'$ into coincidence (Fig. 8.3c). This is the reason why the observed irrational orientation relationship differs from that implied by the Bain strain. The rotation required to convert \mathbf{B} into an ILS precisely corrects the Bain orientation into that which is observed experimentally.

As can be seen from Fig. 8.3c, there is no rotation which can make \mathbf{B} into an invariant-plane strain since this would require two non-parallel invariant-lines. Thus, for the $fcc \rightarrow bcc$ transformation, austenite cannot be transformed into martensite by a homogeneous strain which is an invariant-plane strain. And yet, the observed shape deformation leaves the habit plane undistorted and unrotated, *i.e.*, it is an invariant-plane strain.

The phenomenological theory of martensite crystallography solves this remaining problem (Fig. 8.4). The Bain strain converts the structure of the parent phase into that of the product phase. When combined with an appropriate rigid body rotation, the net homogeneous lattice deformation \mathbf{RB} is an invariant-line strain (step a to c in Fig. 8.4). However, the observed shape deformation is an invariant-plane strain \mathbf{P}_1 (step a to b in Fig. 8.4), but this gives the wrong crystal structure. If a second homogeneous shear \mathbf{P}_2 is combined with \mathbf{P}_1 (step b to c), then the correct structure is obtained but the wrong shape since

$$\mathbf{P}_1\mathbf{P}_2 = \mathbf{RB}.$$

These discrepancies are all resolved if the shape changing effect of \mathbf{P}_2 is cancelled macroscopically

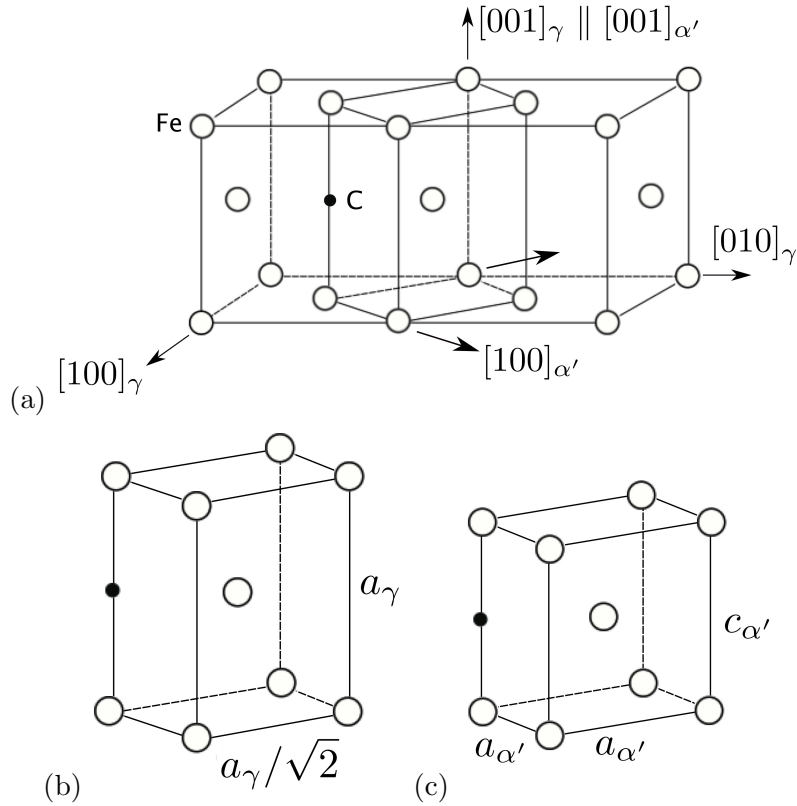


Figure 8.2: The Bain strain. Some of the iron atoms at the face-centres of the austenite cell are omitted for clarity. (a) The lattice correspondence for formation of martensite from austenite, showing a single carbon atom in an octahedral interstice on the $[001]_{\gamma}$ axis. (b) Tetragonal unit cell outlined in austenite. (c) Lattice deformation (compression along c -axis) to form martensite with an appropriate c/a ratio.

by an inhomogeneous lattice-invariant deformation, which may be slip or twinning as illustrated in Fig. 8.4.

The theory explains all the observed features of the martensite crystallography. The orientation relationship is predicted by deducing the rotation needed to change the Bain strain into an invariant-line strain. The habit plane does not have rational indices because the amount of lattice-invariant deformation needed to recover the correct the macroscopic shape is not usually rational. The theory predicts a substructure in plates of martensite (either twins or slip steps) as is observed experimentally. The transformation goes to all the trouble of ensuring that the shape deformation is macroscopically an invariant-plane strain because this reduces the strain energy when compared with the case where the shape deformation might be an invariant-line strain.

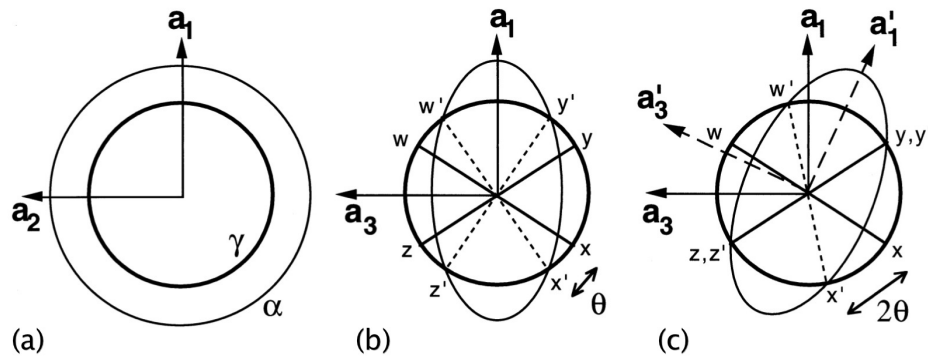


Figure 8.3: (a) and (b) show the effect of the Bain strain on austenite, which when undeformed is represented as a sphere of diameter $wx = yz$ in three-dimensions. The strain transforms it into an ellipsoid of revolution. (c) Shows the ILS obtained by combining the Bain strain with a rigid body rotation through an angle θ . \mathbf{a}_1 , \mathbf{a}_2 and \mathbf{a}_3 refer to $[100]_\gamma$, $[010]_\gamma$ and $[001]_\gamma$ axes respectively.

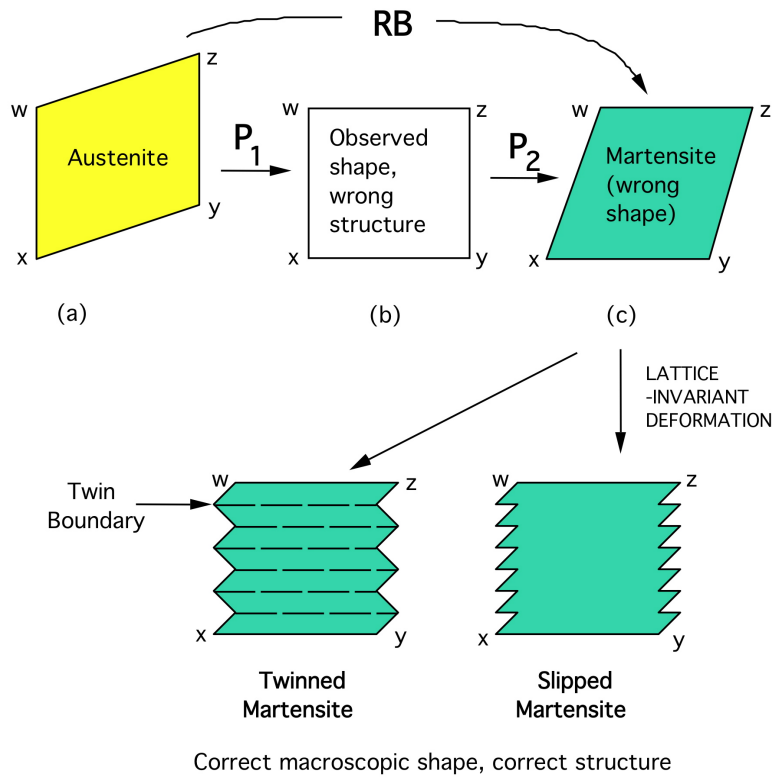


Figure 8.4: The phenomenological theory of martensite crystallography.

Question Sheet 1

1. Draw an accurate 127 mm diameter stereogram of a cubic crystal centred on (001), showing all poles of the form $\{100\}$, $\{110\}$ and $\{111\}$.

A single crystal of copper deforms simultaneously on the slip planes (111) and $(\bar{1}\bar{1}1)$. When dislocations on these planes intersect the free surface they leave the traces of the planes visible on the free surface.

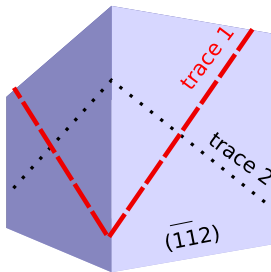


Figure 8.5: Traces on the free surface of a crystal due to slip on two planes. Indicate on your stereogram the traces of the two slip planes and of the plane parallel to the $(\bar{1}\bar{1}2)$ face of the crystal. By finding the intersection of the traces, mark on your stereogram the two directions of the slip planes on $(\bar{1}\bar{1}2)$. Use a Wulff net to determine the angle between these two directions and check by calculation.

2. In an hexagonal crystal the angle $(10\bar{1}0) : (10\bar{1}1)$ is found to be 37.2° . Calculate the ratio c/a . What are the indices of the direction common to these faces, in both three and four index notation?

Show that $(0001) : (11\bar{2}2) = 48.8^\circ$. Draw an accurate 127 mm diameter stereogram centred on 0001 showing all the poles of the form $\{10\bar{1}0\}$, $\{10\bar{1}1\}$, $\{11\bar{2}0\}$, and $\{11\bar{2}2\}$.

3. A tetragonal crystal (point group 422, $a = 1.03$ nm, $c = 0.69$ nm) has faces of the forms $\{100\}$, $\{110\}$, $\{101\}$ and $\{111\}$ as well as an unknown form $\{hkl\}$. One face F of the latter form lies in the same zone as (101) and (110) with $F : (101) = 42^\circ$ and $F : (110) = 25^\circ$.

- Draw a sketch stereogram of the symmetry elements of the group 422 and the poles of the general form $\{hkl\}$.
- Show that $(001) : (101) = 33.8^\circ$. Draw an accurate 127 mm diameter stereogram centred on 001, showing all the faces of the forms listed above. Locate the face F and all its equivalents in the same form.
- Verify that F is (321).

Question Sheet 2

Question 1

A thin film of silver is deposited on to a single-crystal ceramic substrate and their relative orientations measured. Fig. 8.6 shows the 111 poles from the silver together with the 110 poles from the ceramic. Both silver and the ceramic have a cubic lattice, with parameters 0.4086 nm and 0.5760 nm respectively.

Label the poles and determine the orientation relationship. Why might this orientation relationship be adopted?

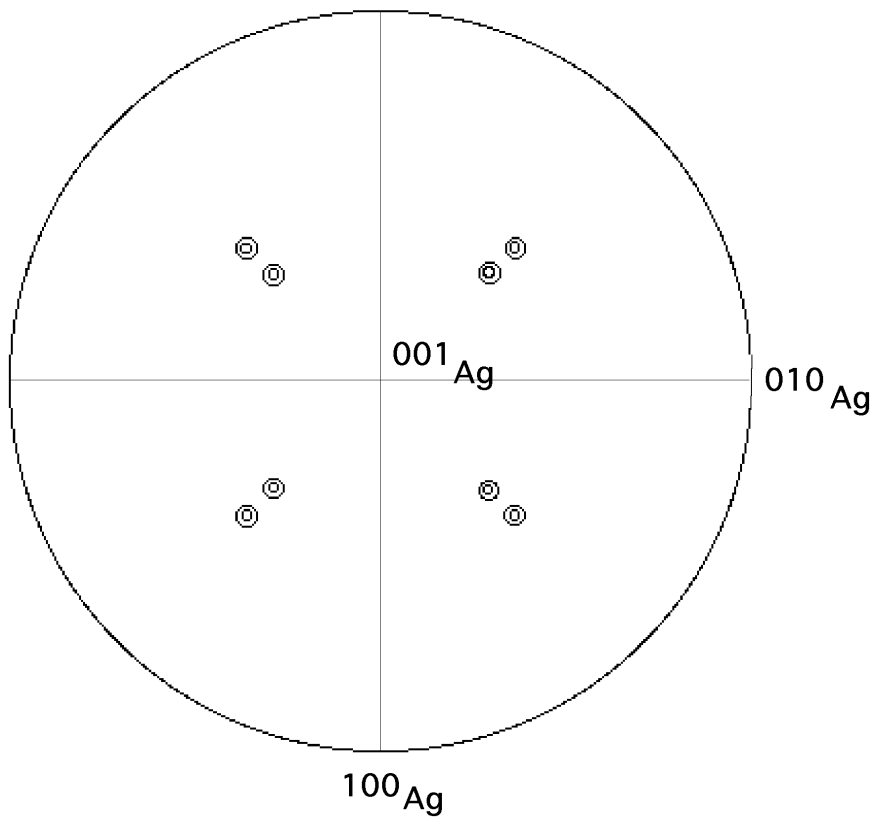


Figure 8.6: Orientation relationship between Ag deposited on to a cubic ceramic substrate.

Question 2

Describe the Ewald sphere construction and using a sketch, explain why in transmission electron microscopy, it is possible to observe diffracted intensity even when the crystal is not exactly at the Bragg orientation.

Figure 8.7 shows an electron diffraction pattern from a body-centred cubic crystal structure. Examine the symmetry of this pattern and deduce the direction of the electron beam. Hence label each of spots on the pattern. Why are some of the spots more intense than others?



Figure 8.7: An electron diffraction pattern from a body-centred cubic crystal.

Question 3

Using real and reciprocal lattice vectors, prove the Weiss zone rule that when a direction with real space indices $[u \ v \ w]$ lies in a plane with reciprocal space indices $(h \ k \ l)$,

$$uh + vk + wl = 0 \quad (8.3)$$

irrespective of the nature of the unit cell.

Question 4

Silicon has a cubic-F lattice with a motif of atoms at $(0,0,0)$ and $(\frac{1}{4}, \frac{1}{4}, \frac{1}{4})$. Draw a projection of the cell and identify on this the diamond glide plane, indicating the translations involved. Indicate a possible Burgers vector of a dislocation whose motion would leave the lattice unchanged.

Question 5

Explain why in Fig. 8.8 there is a central region of strong reflections surrounded by two annular rings. Verify that the electron beam is parallel to a $\langle 210 \rangle$ direction by indexing the spots in the central region.

Show that the radius of the first bright ring in reciprocal space is given by

$$r^* = \sqrt{\left(\frac{1}{\lambda}\right)^2 - \left(\frac{1}{\lambda} - \frac{1}{t}\right)^2} \quad (8.4)$$

where t is the spacing of the planes normal to the $\langle 210 \rangle$ vector.

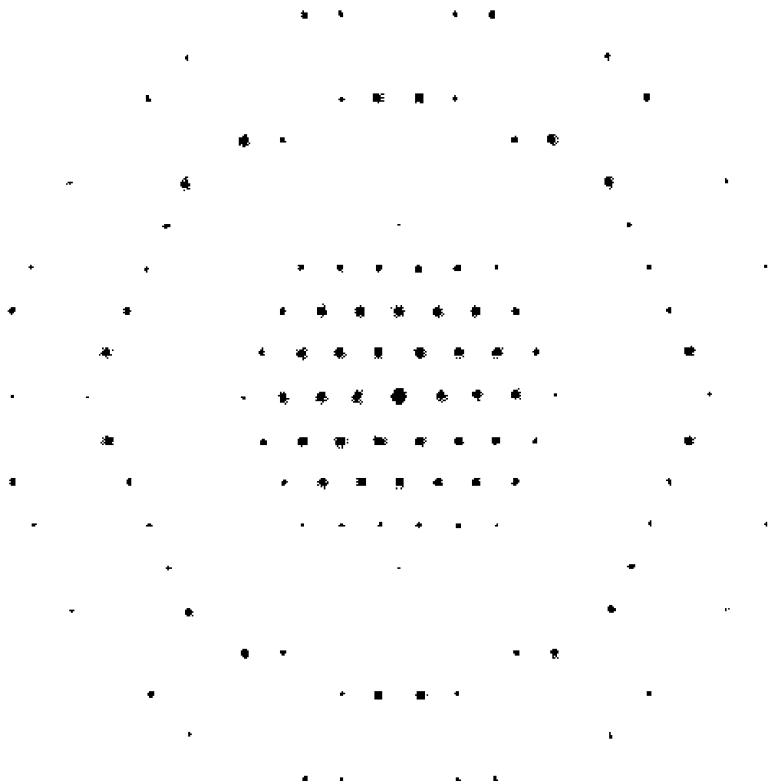


Figure 8.8: Electron diffraction pattern from a cubic-I crystal of lattice parameter 0.89 nm

Examples Class 1

Point groups and consequences

- Draw structure projections of the unit cells of austenite and ferrite, and mark on these the locations of the octahedral interstices.
- Identify the point group symmetry of an octahedral interstice in austenitic iron. Repeat this for the octahedral interstice in ferritic iron. Identify using the table below, the symmetry class to which each interstice belongs.
- Why does carbon strengthen ferrite much more than austenite?

Class	Non-centrosymmetric point groups	Centrosymmetric point groups
Cubic	$23, 432, \bar{4}3m$	$m\bar{3}, m3m$
Hexagonal	$6, \bar{6}, 622, 6mm, \bar{6}m2$	$6/m, 6/mmm$
Trigonal	$3, \bar{3}2, 3m$	$\bar{3}, \bar{3}m$
Tetragonal	$4, \bar{4}, 422, 4mm, \bar{4}2m$	$4/m, 4/mmm$
Orthorhombic	$222, 2mm$	mmm
Monoclinic	$2, m$	$2/m$
Triclinic	1	$\bar{1}$

Sketch Sterograms

The corners of a wooden cube are being cut off to make small equal faces of the form $\{111\}$. The first four new faces are cut in the order (a) (111) ; (b) $(11\bar{1})$; (c) $(\bar{1}11)$ and (d) $(\bar{1}\bar{1}\bar{1})$.

1. Sketch stereographic projections, displaying the faces and the symmetry elements of the model before cutting, and after each new face is made.
2. Using the table of crystal systems in which defining symmetries are given for each crystal system, name the crystal system to which the model will belong after each cut

Table 8.2: The crystal systems

System	Conventional unit cell		Defining symmetry
Triclinic	$a_1 \neq a_2 \neq a_3$	$\alpha \neq \beta \neq \gamma$	monad
Monoclinic	$a_1 \neq a_2 \neq a_3$	$\alpha = \gamma, \beta \geq 90^\circ$	1 diad
Orthorhombic	$a_1 \neq a_2 \neq a_3$	$\alpha = \beta = \gamma = 90^\circ$	3 diads
Tetragonal	$a_1 = a_2 \neq a_3$	$\alpha = \beta = \gamma = 90^\circ$	1 tetrad
Trigonal	$a_1 = a_2 = a_3$	$\alpha = \beta = \gamma \neq 90^\circ$	1 triad
Hexagonal	$a_1 = a_2 \neq a_3$	$\alpha = \beta = 90^\circ, \gamma = 120^\circ$	1 hexad
Cubic	$a_1 = a_2 = a_3$	$\alpha = \beta = \gamma = 90^\circ$	4 triads

Examples Class 2

Calcium Chloride

The orthorhombic unit cell of CaCl_2 has $a = 0.624 \text{ nm}$, $b = 0.643 \text{ nm}$ and $c = 0.420 \text{ nm}$ with ion positions at

$$\text{Ca:} \quad 0,0,0 \quad \frac{1}{2}, \frac{1}{2}, \frac{1}{2}.$$

$$\text{Cl:} \quad x, y, 0 \quad \bar{x}, \bar{y}, 0 \quad \frac{1}{2} + x, \frac{1}{2} - y, \frac{1}{2} \quad \frac{1}{2} - x, \frac{1}{2} + y, \frac{1}{2}$$

with $x = 0.325$ and $y = 0.275$. Fig. 8.9 is an accurate projection of this structure on (001).

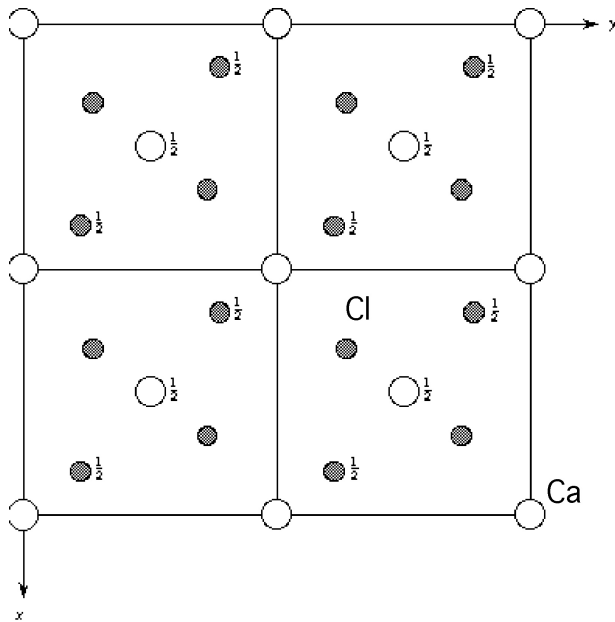


Figure 8.9: The structure projection for calcium chloride

1. What is the Bravais lattice of this structure?
2. Locate all symmetry elements present in the structure and hence determine those along $[100]$, $[010]$ and $[001]$. What is the point group of the crystal structure?
3. Determine the point symmetries of the Ca and Cl ions and express them on sketch stereograms.

Martensite

Show diagrammatically that it is impossible to obtain a fully coherent boundary between austenite and martensite.

Orientation relationships

A rotation matrix can be used to describe the orientation relationship between two grains with identical crystal structure. It can also be described by an axis of rotation and a right-handed angle of rotation (an axis-angle pair).

The general rotation matrix relating the two cubic lattices for a right-handed rotation θ about a unit axis $[u_1 \ u_2 \ u_3]$ is given by:

$$(\text{Y J X}) = \begin{pmatrix} u_1 u_1 (1 - m) + m & u_1 u_2 (1 - m) + u_3 n & u_1 u_3 (1 - m) - u_2 n \\ u_1 u_2 (1 - m) - u_3 n & u_2 u_2 (1 - m) + m & u_2 u_3 (1 - m) + u_1 n \\ u_1 u_3 (1 - m) + u_2 n & u_2 u_3 (1 - m) - u_1 n & u_3 u_3 (1 - m) + m \end{pmatrix} \quad (8.5)$$

where $m = \cos \theta$ and $n = \sin \theta$

Show how you might deduce the axis-angle pair from this matrix. Hence derive the axis-angle pair for the rotation matrix

$$(\text{Y J X}) = \begin{pmatrix} 0 & 1 & 0 \\ \bar{1} & 0 & 0 \\ 0 & 0 & 1 \end{pmatrix} \quad (8.6)$$

What is the Σ value relating these two grains?